The Plant Cell, Vol. 23: 1536–1555, April 2011, www.plantcell.org © 2011 American Society of Plant Biologists

MATE2 Mediates Vacuolar Sequestration of Flavonoid Glycosides and Glycoside Malonates in *Medicago truncatula* [C][W][OA]

Jian Zhao, David Huhman, Gail Shadle, Xian-Zhi He, Lloyd W. Sumner, Yuhong Tang, and Richard A. Dixon[1]

Plant Biology Division, Samuel Roberts Noble Foundation, Ardmore, Oklahoma 73401

The majority of flavonoids, such as anthocyanins, proanthocyanidins, and isoflavones, are stored in the central vacuole, but the molecular basis of flavonoid transport is still poorly understood. Here, we report the functional characterization of a multidrug and toxin extrusion transporter (MATE2), from *Medicago truncatula*. MATE 2 is expressed primarily in leaves and flowers. Despite its high similarity to the epicatechin 3′-*O*-glucoside transporter MATE1, MATE2 cannot efficiently transport proanthocyanidin precursors. In contrast, MATE2 shows higher transport capacity for anthocyanins and lower efficiency for other flavonoid glycosides. Three malonyltransferases that are coexpressed with MATE2 were identified. The malonylated flavonoid glucosides generated by these malonyltransferases are more efficiently taken up into MATE2-containing membrane vesicles than are the parent glycosides. Malonylation increases both the affinity and transport efficiency of flavonoid glucosides for uptake by MATE2. Genetic loss of MATE2 function leads to the disappearance of leaf anthocyanin pigmentation and pale flower color as a result of drastic decreases in the levels of various flavonoids. However, some flavonoid glycoside malonates accumulate to higher levels in *MATE2* knockouts than in wild-type controls. Deletion of MATE2 increases seed proanthocyanidin biosynthesis, presumably via redirection of metabolic flux from anthocyanin storage.

INTRODUCTION

Anthocyanins and proanthocyanidins (PAs; also called condensed tannins) are abundant flavonoids found in seed coats, leaves, fruits, flowers, and bark of many plant species (Ariga et al., 1981; Gabetta et al., 2000; Gu et al., 2004; Dixon et al., 2005). PAs and anthocyanins play protective roles against microbial pathogens, insect attack, and UV irradiation, and anthocyanins are commonly utilized to attract insect pollinators. For humans, both classes of compounds have beneficial effects on cardiac health, immunity, and longevity (Santos-Buelga and Scalbert, 2000; Skibola and Smith, 2000), and the presence of modest levels of PAs in the leaves and stems of protein-rich forage crops is an important agronomic trait, as they protect ruminant animals from pasture bloat, enhance ruminant nutrition, and reduce protein degradation in silage (Lees, 1992).

Attempts to engineer PA production in the forage legume alfalfa (*Medicago sativa*) have so far led to the accumulation of anthocyanins rather than PAs (Peel et al., 2009). Flavan 3-ol-derived PA oligomers and anthocyanins are derived from the same precursors, anthocyanidins, and competition between these parallel pathways for metabolic flux might be an important regulatory mechanism determining PA biosynthesis (Lepiniec et al., 2006; Figure 1). Anthocyanidins (such as cyanidin, pelargonidin, and delphinidin) from the flavonoid pathway can be either immediately modified by glycosylation, acylation, and/or methylation to generate diverse anthocyanins or further reduced to generate flavan 3-ol precursors of PAs, such as epicatechin formed by the action of anthocyanidin reductase (ANR; Figure 1; Xie et al., 2003). Seeds of knockout mutants in *ANR* accumulate many more anthocyanins than wild-type seeds (Marinova et al., 2007b), and an inverse relationship between the expression of *ANR* and *anthocyanidin 3-O-glucosyltransferase* has been demonstrated for selective direction of cyanidin into either PA or anthocyanin biosynthesis (Lee et al., 2005).

The family I glycosyltransferases UTG78G1 and UTG72L1 catalyze the glucosylation of anthocyanidins and epicatechin, respectively (Modolo et al., 2007; Pang et al., 2008; Peel et al., 2009). Glycosylation of epicatechin and cyanidin is essential for their transport into the vacuole by the multidrug and toxin extrusion transporters MATE1 and TT12 in the seed coats of *Medicago truncatula* and *Arabidopsis thaliana*, respectively (Marinova et al., 2007b; Zhao and Dixon, 2009; Figure 1). Many flavonoid glycosides accumulate in the vacuole with acyl substituents on the sugar residues, but the exact function of the acylation remains unclear. Whereas acylation with malonyl residues has been suggested to be essential for the retention of some glycosides within the vacuole (Matern et al., 1983), other studies indicate the involvement of acylation in flavonoid transport per se. For example, proton gradient–dependent vacuolar uptake by unknown transporters of anthocyanidin-3-*O*-sinapoyl

[1] Address correspondence to radixon@noble.org.
The author responsible for distribution of materials integral to the findings presented in this article in accordance with the policy described in the Instructions for Authors (www.plantcell.org) is: Richard A. Dixon (radixon@noble.org).
[C]Some figures in this article are displayed in color online but in black and white in the print edition.
[W]Online version contains Web-only data.
[OA]Open Access articles can be viewed online without a subscription.
www.plantcell.org/cgi/doi/10.1105/tpc.110.080804

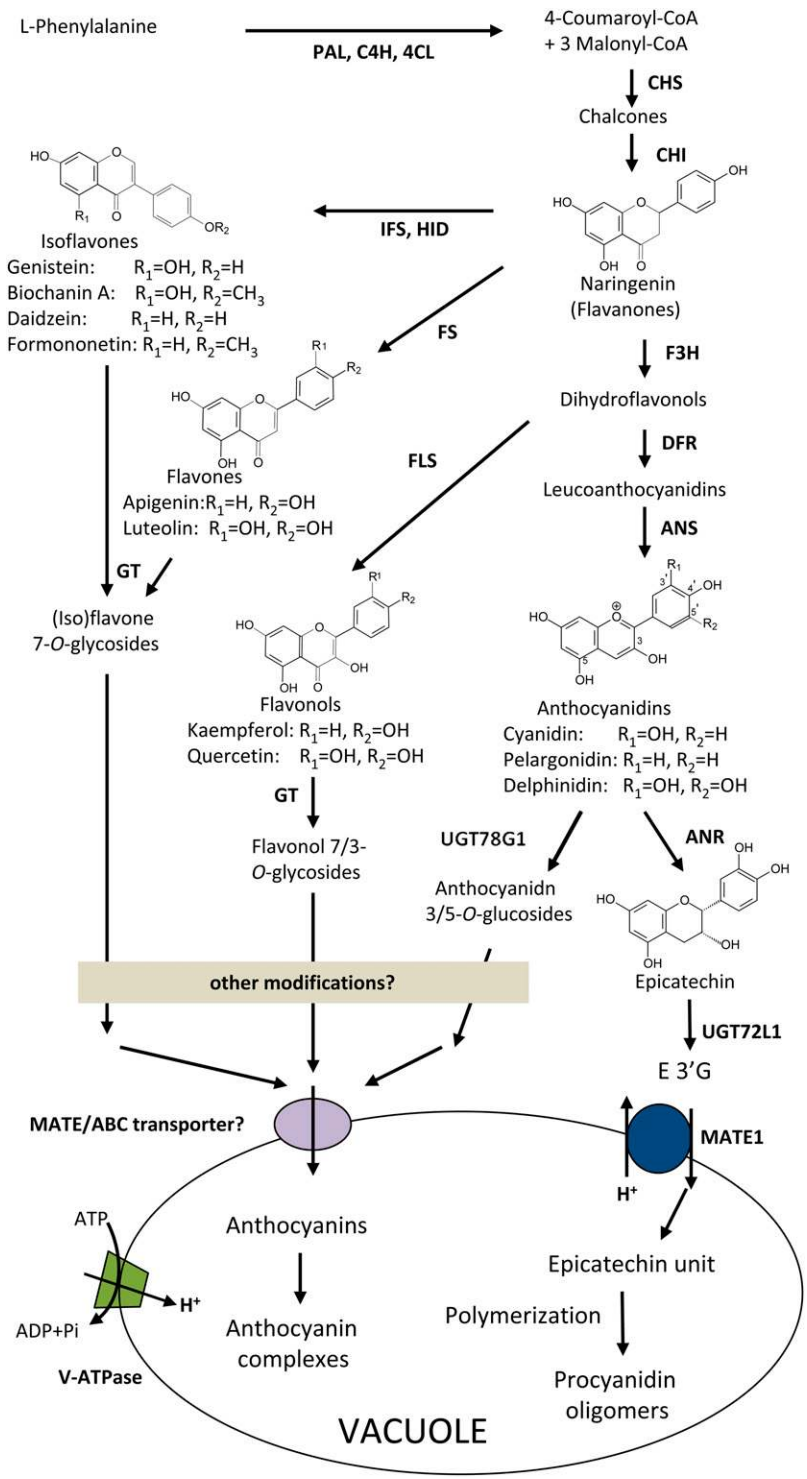

Figure 1. Pathways for Flavonoid Synthesis, Modification, and Transport.

Enzymes are as follows: PAL, L-Phe ammonia-lyase; C4H, cinnamate 4-hydroxylase; 4CL, 4-coumarate:CoA ligase; CHS, chalcone synthase; CHI, chalcone isomerase; F3H, flavanone 3-hydroxylase; DFR, dihydroflavonol reductase; FS, flavone synthase; IFS, isoflavone synthase; HID, 2-hydroxyisoflavanone dehydratase; FLS, flavonol synthase; ANS, anthocyanidin synthase; ANR, anthocyanidin reductase; GT, glycosyltransferase; MaT, malonyl CoA:flavonoid acyltransferase; MATE, multidrug and toxin extrusion transporter; V-ATPase, vacuolar ATPase.
[See online article for color version of this figure.]

xyloseglucosylgalactoside or apigenin 7-*O*-(6′′-*O*-malonylglucoside) strongly depended on acylation of the attached sugars (Matern et al., 1986; Hopp and Seitz, 1987). Biochemical studies of other vacuolar transport systems for flavonoids have not led to a consistent view of the substrate specificity requirements (Klein et al., 1996, 2000; Bartholomew et al., 2002; Frangne et al., 2002).

The ATP binding cassette (ABC) transporter MRP3 from maize (*Zea mays*; Goodman et al., 2004), the MATE transporters AM1 and AM3 from grapevine (*Vitis vinifera*; Gomez et al., 2009), and FFT from *Arabidopsis* (Thompson et al., 2010) were suggested to be involved in anthocyanin/flavonol transport. However, due to the lack of complete data sets on transport properties, substrate preferences, in vivo substrates, or genetically determined in planta functions for each of these transporters, our overall picture of flavonoid transport is still incomplete. The study of intercellular or subcellular transport and storage of plant specialized metabolites, including flavonoids, has emerged as an important and rapidly growing area and is expected to have major impacts on our understanding of plant specialized metabolism and metabolic engineering (Zhao and Dixon, 2010).

During our studies on the tonoplast epicatechin 3′-*O*-glucoside (E3′G) transporter MATE1 (Zhao and Dixon, 2009), we identified another transporter, MATE2, based on homology to *Arabidopsis* TT12. Here, we report that MATE2 is a flavonoid transporter with a wide substrate spectrum. This vacuolar transporter can transport flavonoid glycosides, particularly anthocyanin and flavone glucosides. However, MATE2 prefers to transport malonylated flavonoid glucosides. The flavonoid malonylation reaction is performed by three malonyl CoA:flavonoid malonyltransferases, encoded by genes that are coexpressed with MATE2 in *M. truncatula* tissues. Characterization of *mate2* knockout mutants confirms that MATE2 is a flavonoid transporter involved in vacuolar sequestration of anthocyanins and other flavonoids in flowers and leaves.

RESULTS

Identification of *Medicago* MATE2

During characterization of MATE1 as the tonoplast transporter for E3′G (Zhao and Dixon, 2009), we found six related putative transporter proteins by BLAST analysis of the *M. truncatula* genome sequence with the *Arabidopsis* TT12 protein sequence. Of these, only one, designated MATE2, showed uptake activity for flavonoids when expressed in yeast (see below). MATE2 shares 54 and 50% amino acid sequence similarity with MATE1 and TT12, respectively (see Supplemental Figure 1 online). BLAST and sequence alignment of MATE2 with several characterized MATE transporters from other species, however, indicated that *Medicago* MATE2 is more similar to the tomato (*Solanum lycopersicum*) MATE transporter MTP77 (66% identity and 80% similarity), the *Arabidopsis* putative MATE transporter At4g25640 (65% identity and 79% similarity), and the two grapevine MATE transporters AM3 (62% identity and 79% similarity) and AM1 (61% identity and 79% similarity) than to *Medicago* MATE1 and TT12 (see Supplemental Figure 1 online). All of these reported MATE transporters are confirmed or putative flavonoid transporters (Mathews et al., 2003; Marinova et al., 2007b; Gomez et al., 2009; Zhao and Dixon, 2009; Thompson et al., 2010). To further predict and distinguish MATE2 function, phylogenetic analysis was performed with protein sequences of different types of known and putative MATE transporters (Supplemental Data Set 1). These proteins grouped into three clades (Figure 2A). The first clade includes three subclades: one contains MATE2 as well as other known anthocyanin/flavonoid MATE transporters; whereas *Medicago* MATE1, *Arabidopsis* TT12, and their putative grapevine and canola (*Brassica napus*) orthologs are grouped into another subclade; and two vacuolar tobacco (*Nicotiana tabacum*) nicotine transporters, Nt MATE1/2 (Shoji et al., 2009), form the third subclade. The nicotine transporter JAT1 from tobacco along with ALF5 and the toxin exporter DTX1 from *Arabidopsis* (Diener et al., 2001; Li et al., 2002; Morita et al., 2009) are grouped together in an independent clade. Three plasma membrane–localized organic acid exporters, Sb MATE1 from sorghum (*Sorghum bicolor*), Hv AACT1 from barley (*Hordeum vulgare*), and FRD3 from *Arabidopsis* (Durrett et al., 2007; Furukawa et al., 2007; Magalhaes et al., 2007), are grouped with their *Medicago* counterpart AC122162_1.4 into a clade much further from the secondary metabolite MATE transporters. The *Arabidopsis* MATE transporter EDS5 is in a separate clade (Nawrath et al., 2002). The phylogenetic analysis suggested that MATE2 may function as a flavonoid transporter, possibly associated with the transport of anthocyanins or flavonols.

MATE2 Transports a Wide Range of Flavonoid Glucosides

MATE2 was expressed in yeast for comparison of substrate transport preference to that of MATE1, which transports both E3′G and cyanidin 3-*O*-glucoside (Cy3G), but with a strong kinetic preference for E3′G (Zhao and Dixon, 2009). Isolated microsomes from yeast cells expressing MATE2 took up Cy3G, whereas uptake by microsomes from vector control cells was significantly less (Figure 2B; see Supplemental Figure 2 online). Similar to MATE1, MATE2-expressing membrane vesicles did not show significant transport activity toward cyanidin, epicatechin, or other flavonoid aglycones (see Supplemental Figure 2 online).

Inhibitors of the vacuolar H^+-ATPase or uncouplers of the proton motive force (Luvisetto and Azzone, 1989; Dröse and Altendorf, 1997; Rodrigues et al., 1999) inhibited Cy3G transport, indicating that MATE2-mediated Cy3G transport is H^+-gradient dependent, as is transport of E3′G by MATE1 (Zhao and Dixon, 2009; Figure 2C). Furthermore, MATE2 was not inhibited by the ATPase inhibitor vanadate, which preferentially inhibits ABC transporters (Pezza et al., 2002).

Of 10 flavonol, flavone, and isoflavone glucosides tested as potential substrates for MATE2, apigenin 7-*O*-glucoside (A7G) exhibited the highest uptake, but this was less than that of Cy3G (Figures 2D and 2E). In particular, MATE2 appears not to transport E3′G, which is the preferred substrate for MATE1 (Figure 2D). In competition assays, A7G, naringenin 7-*O*-glucoside, luteolin 7-*O*-glucoside, and pelargonidin 3-*O*-glucoside (P3G; all at 250 μM) were most effective in inhibiting the uptake of Cy3G (at 100 μM), whereas E3′G and isoflavone glycosides did not

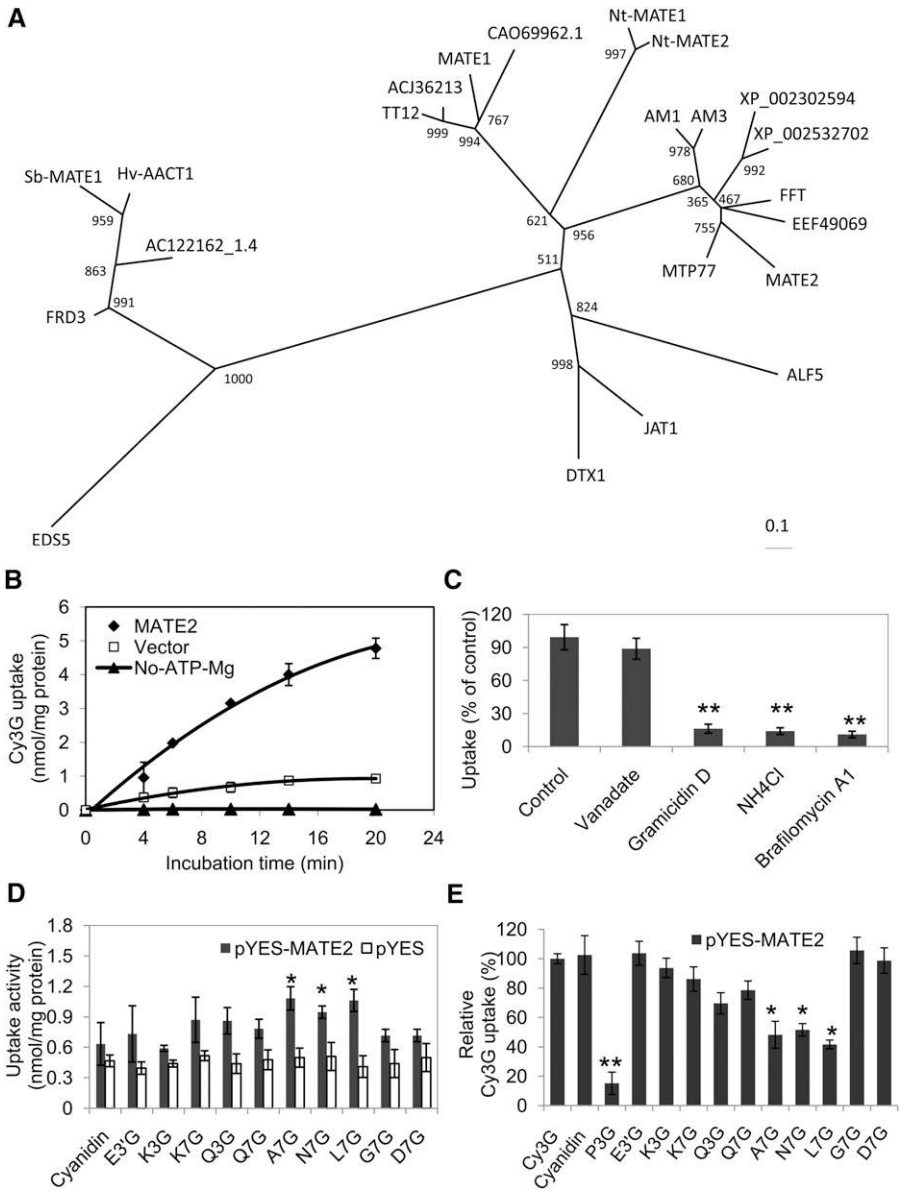

Figure 2. Phylogeny and Transport Activity of MATE2.

(A) Phylogenetic tree of MATE transporters. Protein sequences of the characterized MATE transporters from *Arabidopsis*, TT12, FFT, FRD3, ALF5, EDS5, and DXT1; *M. truncatula* MATE1 and MATE2; sorghum Sb MATE1; grapevine AM1 and AM3; tomato MTP77; barley Hv AACT1; tobacco JAT1, Nt MATE1, and Nt MATE2; as well as predicted MATE transporters CAO69962 (grapevine), ACJ36213 (*Brassica rapa*), XP_002302594 (*P. trichocarpa*), XP_002532702 and EEF49069 (*R. communis*), ACJ36213 (*B. rapa*), and AC122162_1.4 (*M. truncatula*) were aligned with ClustalW, and the nonrooted neighbor-joining tree was generated by the PAUP 4.0 program. Numbers at branch points indicate bootstrap support.

(B) Time-dependent uptake of Cy3G into vacuolar vesicles prepared from yeast cells expressing MATE2 or empty vector. Substrate concentration was 100 μM. Results are means and SD of five replicate uptake assays after subtracting background.

(C) Inhibition of Cy3G uptake (100 μM, 8-min incubation) by inhibitors of membrane transport. Results are means and SD of five replicate uptake assays after subtracting background.

(D) Uptake of other flavonoid glycosides into MATE2-expressing membrane vesicles. Data show ATP-dependent uptake of each flavonoid glycoside or cyanidin (100 μM) by subtracting the −Mg-ATP control background. Flavonoids are as follows: epicatechin 3′-*O*-glucoside (E3′G), kaempferol 3-*O*-glucoside (K3G), kaempferol 7-*O*-glucoside (K7G), apigenin 7-*O*-glucoside (A7G), luteolin 7-*O*-glucoside (L7G), naringenin 7-*O*-glucoside (N7G), quercetin 3-*O*-glucoside (Q3G), quercetin 7-*O*-glucoside (Q7G), daidzein 7-*O* glucoside (D7G), genistein 7-*O*-glucoside (G7G), and pelargonidin 3-*O*-glucoside (P3G).

(E) Competition by various flavonoids for uptake of Cy3G (50 μM) by MATE2. Cy3G uptake without competitor (3 nmol/mg protein over 8 min) was set as 100%. Relative Cy3G uptake in the presence of other flavonoids (250 μM) is shown after subtraction of background. Results are means and SD of three replicate uptake assays.

Asterisks indicate statistically significant differences (** $P < 0.01$, * $P < 0.05$, paired *t* test) compared with corresponding controls (pYES vector control or 100% Cy3G uptake).

cause inhibition (Figure 2E). Overall, the data suggest that MATE2 can transport a wide range of flavonoids, including anthocyanins and flavone glycosides, albeit with different efficiencies.

Tissue-Level Expression of MATE2 and Flavonoid Modification Genes

Mining microarray data from the *Medicago* Gene Expression Atlas (MtGEA) database (http://mtgea.noble.org/v2/; Benedito et al., 2008) showed that *MATE2* is most strongly expressed in flowers, followed by roots and vegetative buds, leaves, and seeds (see Supplemental Figure 3 online). Since MATE2 transports glycosylated flavonoids rather than flavonoid aglycones, flavonoid glycosyltransferases may be spatially coexpressed with *MATE2*. *UGT78G1*, previously identified as a *Medicago* anthocyanidin glycosyltransferase (Modolo et al., 2007; Peel et al., 2009), shows a similar tissue expression pattern to that of *MATE2*, being highly expressed in pod, flower, vegetative bud, root, and leaf tissues (see Supplemental Figure 3 online). To further examine genes coexpressed with *MATE2* and *UGT78G1*, hierarchical clustering was conducted based on Pearson correlation of expression data from the MtGEA, and a coregulated group of genes involved in flavonoid biosynthesis, modification, and transport was generated (Figure 3A; see Supplemental Figure 4 online). Two major clusters were identified based on these data: genes involved in the early steps and genes involved in the later steps of flavonoid biosynthesis. The effectiveness of clustering is shown by coclustering of *ANS*, *ANR*, and *UGT72L1* involved in the PA biosynthesis pathway (Xie et al., 2003; Pang et al., 2008). The coordinated expression patterns of *MATE2* and *UGT78G1* are consistent with their functional corelationship. Interestingly, two putative malonyltransferases (probe sets Mtr.19777.1.S1_at and Mtr.19945.1.S1_at, named *MaT4* and *MaT5*, respectively) also clustered with these flavonoid biosynthesis, modification, and transport genes (Figure 3A). Malonylation is a major modification on anthocyanins and (iso)flavonoid glycosides in *M. truncatula* (Farag et al., 2008); and the expression patterns therefore suggested that these malonyltransferases might be involved in the modification of flavonoid glucosides.

Quantitative RT-PCR analysis of flavonoid biosynthesis–related genes indicated that most genes showed diverse tissue expression patterns, presumably because of the complex and widespread accumulation of (iso)flavonoid compounds in *M. truncatula* (see Supplemental Figure 3 online). However, UGT78G1, MaT4, MaT5, and MATE2 are all expressed in flower, root, and leaf to varying levels (Figure 3B). Examination of the developmental stage–dependent expression of *MATE2* indicated strong expression in flowers compared with vegetative buds and leaves (Figure 3C). To further examine the cell type expression of *MATE2*, in situ hybridization was conducted with both floral and leaf tissues. Consistent with the RT-PCR data, *MATE2* transcripts showed higher signal intensity in younger flower and leaf tissues than in older tissues (Figure 3D). *MATE2* signal was mainly in the mesophyll cells of young leaves but was evenly distributed throughout the cells of the vegetative bud. In cross sections of young flowers, although the petals and pollen were labeled, the strongest signals were in the outer petals and sepals of the flower. In cross sections of the petals of fully opened flowers, *MATE2* transcript signal was strong in both epidermal cells and vascular bundles of veins (Figure 3D).

Malonyltransferases Modify Flavonoid Glucosides

Based on the above expression patterns, we selected and cloned the putative malonyltransferases to test their functions. Because the transport efficiency of MATE2 toward anthocyanins and flavonol glucosides is lower than that of other MATE transporters, such as MATE1 toward E3′G (Zhao and Dixon, 2009), we also tested whether flavonoid glucoside malonates generated by the action of these enzymes would be better substrates for MATE2 transport than are the nonsubstituted glycosides. For this purpose, we also cloned a third putative malonyltransferase, MaT6, which is weakly expressed in leaf and root (Figure 3) but was not represented on the *Medicago* Affymetrix gene chip.

Protein sequence alignment showed that MaT4, MaT5, and MaT6 not only have the HXXXD and DFGWG domains that are conserved in all BAHD (for BEAT, AHCTs, HCBT, and DAT; St. Pierre and De Luca, 2000) family proteins but also have the conserved NYXGNC domain found only in malonyl CoA:flavonoid malonyltransferases (see Supplemental Figure 5 online). Phylogenetic analysis showed that MaT4 to -6, MaT1 to -3, and other anthocyanin and flavonoid malonyltransferases are clustered into the same clade (Figure 4A), while other putative malonyltransferases from *M. truncatula* are separated from the known flavonoid malonyltransferases (Supplemental Data Set 2).

Recombinant His-tagged MaT4 to -6 proteins were expressed in *Escherichia coli*, purified on a nickel-resin column (Figure 4B), and examined for in vitro malonyltransferase activity. Using the aliphatic thioester donors malonyl CoA and acetyl CoA or the aromatic acyl donor *p*-coumaroyl-CoA in combination with flavonoid glucosides as acceptors, each of the three MaTs showed different substrate preferences and donor specificities (Figures 4C to 4N). All three enzymes used only malonyl CoA to acylate their preferred substrates (see Supplemental Table 1 and Supplemental Figure 5 online). MaT4 prefers to acylate 7-*O* glucosides, including isoflavone, flavonol, or flavanone 7-*O*-glucosides, but shows little activity toward 3-*O*-glucosides (see Supplemental Table 1 and Supplemental Figure 6 online). MaT5 and MaT6 have similar activity toward anthocyanins (cyanidin, delphinidin, and pelargonidin conjugates) and exhibit a regiospecific preference for 3-*O*-glucosides, with less activity with 3,5-di-*O*-glucosides (see Supplemental Table 1 and Supplemental Figure 7 online). Electrospray ionization-liquid chromatography-mass spectrometry (ESI-LC-MS) profiling of the reaction products revealed that MaT4 converts isoflavone and flavanone 7-*O*-glycosides into the corresponding monomalonylated products (see Supplemental Figure 8 online). Although identification of the position of malonylation of the sugar is beyond the scope of this study, it is likely that the products are the flavonoid 7-*O*-(6′′-*O*-malonyl)-β-D-glucosides, with the malonate moiety at the same position on the sugar as in the compounds generated by the *M. truncatula* MaT1, MaT2, and MaT3 malonyltransferases (Yu et al., 2008; see Supplemental Figure 9 online). The reaction product displayed a UV spectrum similar to that of its parental substrate and a mass increment of 86 m/z, the mass

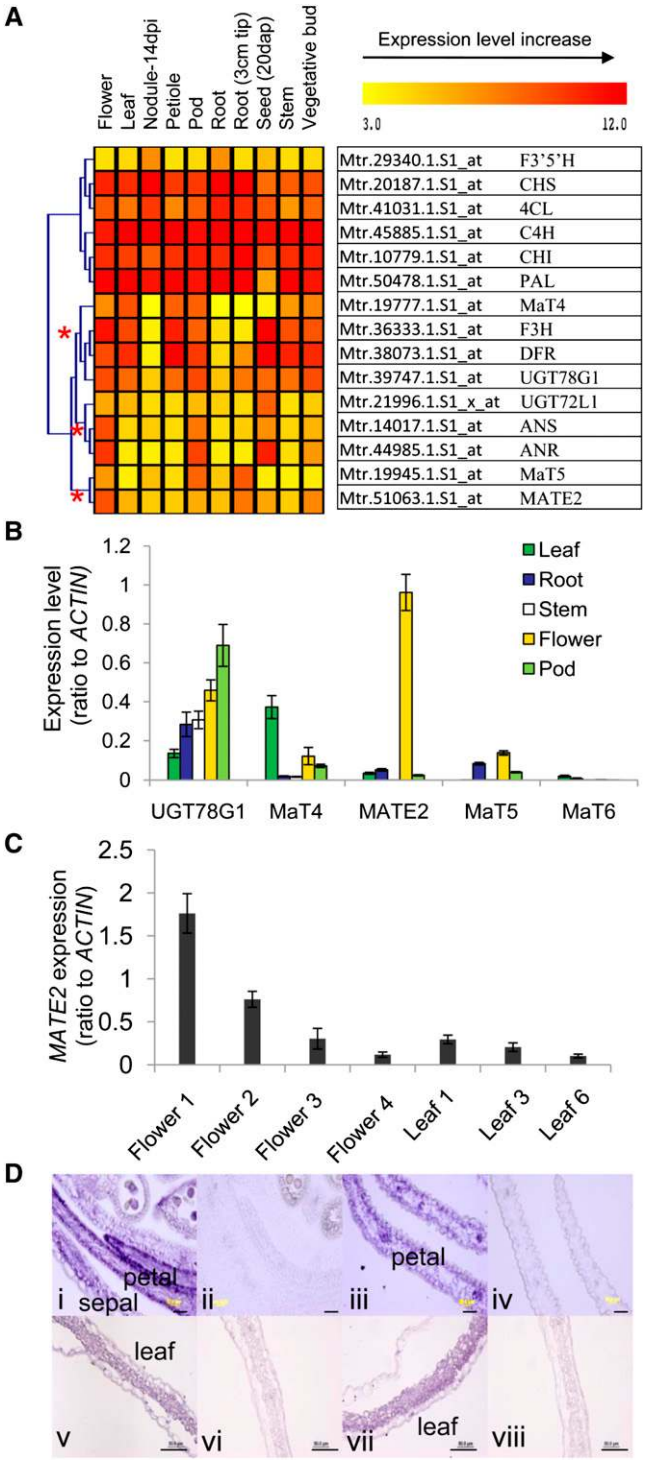

Figure 3. Expression Patterns of *MATE2* and Malonyltransferases in *M. truncatula*.

(A) Coexpression analysis of flavonoid biosynthetic genes with *UGT78G1* and *MATE2*. Gene expression data from the GeneAtlas database (http://mtgea.noble.org/v2/) were $\log_2$ transformed, and hierarchical clustering was conducted based on Pearson correlation. Roots indicated by asterisks show the subclades of significant probability (>95%) calculated by Pvclust (Suzuki and Shimodaira, 2006). Gene names for probe sets are abbreviated as in Figure 1. A heat map mosaic representation of Pearson correlation values between each gene is shown in Supplemental Figure 4 online.

(B) Tissue-level expression pattern of *MATE2* in *M. truncatula*. Quantitative RT-PCR was conducted with mRNA samples from *M. truncatula* leaf (3–4 weeks old), root, stem (five to six internodes from top), vegetative bud, flower (2 d after opening of petals), and pod (6–12 d post-flowering). Amplified genes are shown. *ACTIN* was used as a control. Data are means and SD of triplicate experiments.

(C) Quantitative RT-PCR confirmation of *MATE2* expression in flowers (1–4 d after opening of petals) and leaves (1, 3, and 6 weeks old). Data are means and SD of triplicate experiments.

(D) Cell type expression of *MATE2* in young leaf and flower tissues as shown by in situ hybridization. **(i)** and **(iii)** show *MATE2* expression in epidermal cells of sepals and petals at 3 and 2 d before flower opening, respectively. **(v)** and **(vii)** show *MATE2* transcript signals in young leaf mesophyll cells. **(ii)**, **(iv)**, **(vi)**, and **(viii)** are the corresponding sense controls. Bars = 70 μm.

of the malonyl group. However, MaT5- and MaT6-catalyzed malonylation of anthocyanins was more complex: multiple malonylation products were obtained with five different anthocyanins, with the anthocyanidin glycoside monomalonate and dimalonate being the dominant products (see Supplemental Figure 9 online).

MATE2 Prefers to Transport Malonylated Flavonoids

MATE2 exhibits a K_m of 88.9 μM and a V_{max} of 0.91 nmol/mg protein/min for the uptake of Cy3G (Table 1; see Supplemental Figure 10 online). MATE2 also mediates the uptake of other anthocyanidin glucosides, such as delphinidin 3-*O*-glucoside (D3G; K_m of 96.5 μM and V_{max} of 0.95 nmol/mg protein/min), delphinidin 3,5 di-*O*-diglucoside, P3G, and pelargonidin 3,5-di-*O*-diglucoside (Table 1; see Supplemental Figure 10 online).

To determine whether MATE2 prefers to transport malonylated compared with nonmalonylated flavonoids, we performed uptake assays using pure compounds (A7G and K7G and their malonates A7GM and K7GM) or mixtures of malonylated and nonmalonylated substrates generated from the MaT5 assays (Cy3G and P3G and their malonates Cy3GM and P3GM). The mixtures were used because of the instability of the anthocyanidin malonyl glycosides during purification. In these latter assays, the relative proportions of the two types of compound were compared in the original mixture and the fraction extracted from the MATE2-containing yeast membrane vesicles. MATE2 took up more than five times more A7G malonate than A7G and about two times more kaempferol 7-*O*-glucoside (K7G) malonate than nonmodified K7G (Figures 5A and 5B), suggesting that the transporter preferentially takes up flavonoid glucoside malonates rather than the unsubstituted glycosides. This was confirmed by kinetic analysis (Table 1; see Supplemental Figure 11 online). MATE2 also took up more malonylated anthocyanins, Cy3G and P3G malonates, than nonmodified Cy3G and P3G from malonylation reaction mixtures in standard uptake assays with yeast microsomes (Figures 5C and 5D). Although kinetic parameters for Cy3GM and P3GM uptake could not be

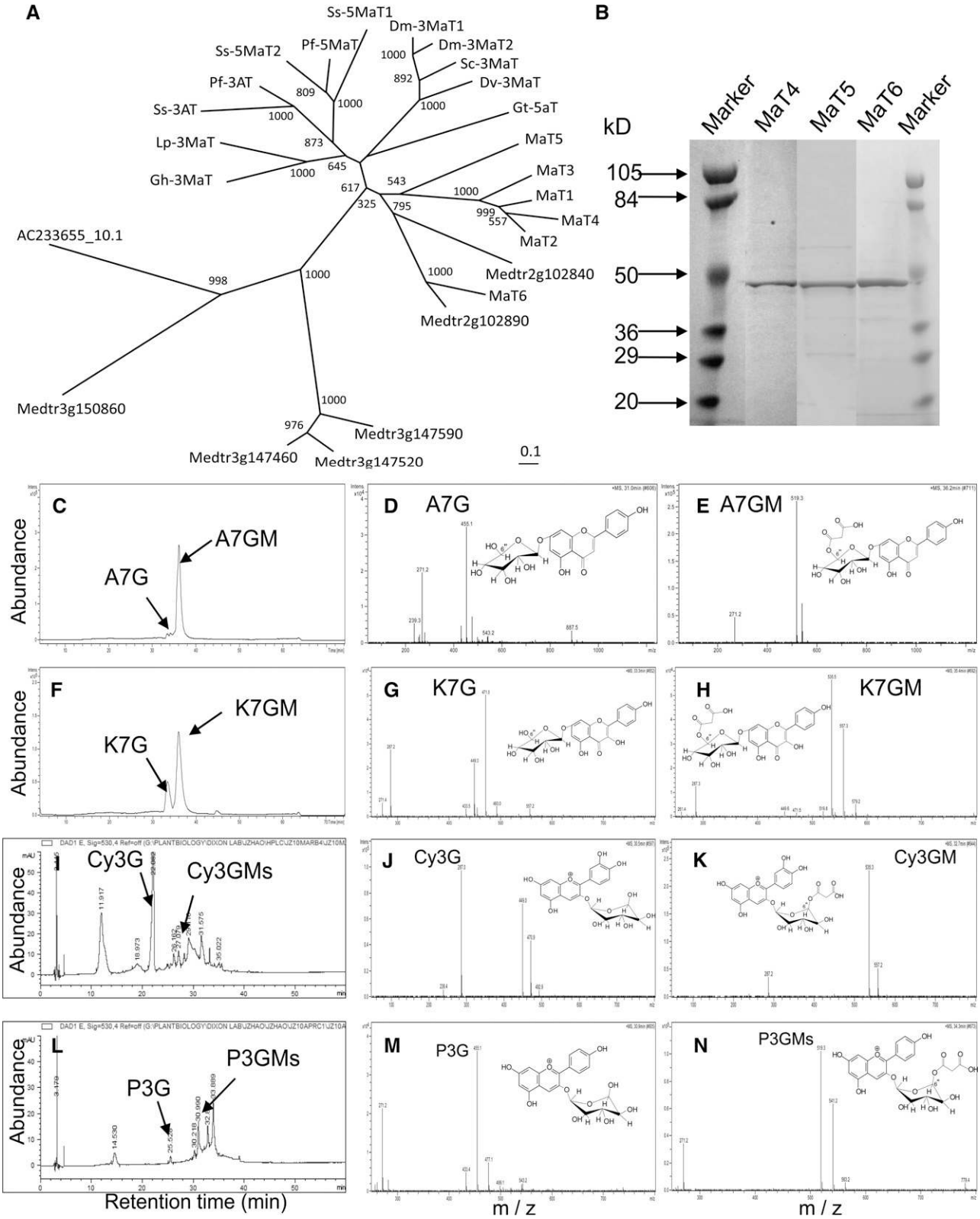

Figure 4. Phylogeny and Activity of *Medicago* Malonyltransferases.

(A) Phylogenetic tree of flavonoid acyltransferase proteins. The lengths of the lines indicate the relative distances between nodes on the nonrooted

Table 1. Kinetic Parameters for *MATE2*-Mediated Uptake of Flavonoid Glucosides and Glucoside Malonates

Flavonoids	K_m (μM)	V_{max} (nmol/mg protein/min)
Cyanidin 3-*O*-glucoside (Cy3G)	88.9 ± 6.8	0.9 ± 0.1
Pelargonidin 3-*O*-glucoside (P3G)	128.8 ± 15.2	0.7 ± 0.1
Pelargonidin 3,5-*O*-diglucoside (P35G)	105.3 ± 9.1	0.8 ± 0.1
Delphinidin-3-*O*-glucoside (D3G)	96.5 ± 5.5	1.0 ± 0.1
Delphinidin-3,5-*O*-diglucoside (D35G)	83.5 ± 9.8	1.0 ± 0.1
Apigenin 7-*O*-glucoside (A7G)	153.1 ± 11.2	8.5 ± 0.1
Apigenin 7-*O*-glucoside malonate (A7GM)	46.2 ± 2.3	26.4 ± 3.4
Kaempferol 7-*O*-glucoside (K7G)	268.0 ± 34.2	7.4 ± 1.1
Kaempferol 7-*O*-glucoside malonate (K7GM)	100.5 ± 12.1	8.5 ± 1.0

determined due to instability and multiple malonylation reaction products with anthocyanins, the mixed substrate competition uptake assays with malonylation reaction mixtures suggested that MATE2 has a kinetic preference for malonylated anthocyanins over the nonmodified glycosides (Figures 5C and 5D).

MATE2 Is a Tonoplast Transporter, Whereas Flavonoid Malonyltransferases Are Cytosolic or Endoplasmic Reticulum Proteins

Several known flavonoid MATE transporters, including AM1, AM3, MATE1, and TT12, are localized to the tonoplast membrane, as shown by imaging of green fluorescent protein (GFP)-tagged transporters or membrane proteomics studies (Marinova et al., 2007a; Gomez et al., 2009; Zhao and Dixon, 2009). Topological prediction suggests that MATE2 has 12 putative transmembrane domains in the same pattern as other known MATE transporters (see Supplemental Figure 12 online). To further determine the subcellular localization of MATE2 protein, a GFP fusion to the C terminus of MATE2 was constructed and expressed in both yeast and plant cells. This GFP fusion protein was competent in anthocyanin transport when expressed in yeast microsomes (see Supplemental Figure 13A online). When driven by the glyceraldehyde 3-phosphate dehydrogenase promoter in yeast cells, MATE2-GFP localized to the tonoplast, as indicated by the ring-like endomembrane structure labeled with the MATE-GFP fluorescence signal (see Supplemental Figure 13B online). The MATE2-GFP–labeled endomembranes cofractionated with vacuolar membrane–enriched fractions on sucrose-density gradient centrifugation (see Supplemental Figure 13C online). Similarly, MATE2-GFP localized to vacuolar membranes when 35S promoter–driven MATE2-GFP constructs were stably expressed in *Arabidopsis* (Figure 6; see Supplemental Figure 14 online). MATE2-GFP appeared to label both vacuolar membranes and membrane structures between the vacuole and the nucleus in *Arabidopsis* epidermal cells (Figures 6A to 6C). When compared with chloroplast autofluorescence in *Arabidopsis* petiole cells expressing MATE2-GFP, MATE2-GFP–labeled endomembranes were clearly interior to chloroplasts, suggesting that the MATE2-GFP–labeled endomembrane is the vacuolar membrane rather than the plasma membrane (Figures 6A to 6C). This conclusion was further strengthened by comparison of the MATE2-GFP fluorescence pattern in *Arabidopsis* petiole cells in which the plasma membrane had been labeled with the red fluorescent dye FM4-64 (Figures 6D to 6F). The FM4-64–labeled plasma membrane was external to the MATE2-GFP–labeled vacuolar membrane. Similar vacuolar membrane localization was also seen when MATE2-GFP was expressed in onion (*Allium cepa*) and tobacco epidermal cells, compared with the general distribution of free GFP control (see Supplemental Figure 14 online).

The three malonyltransferases MaT4, MaT5, and MaT6 were also fused to GFP for determination of their subcellular

Figure 4. (continued).

neighbor-joining tree. Numbers at branch points indicate bootstrap support. Proteins and their accession numbers are given in Methods. Putative acyltransferases Medtr3g150860, Medtr3g147460, Medtr3g147520, Medtr3g147590, Medtr2g102890, Medtr2g102840, and AC233655_10.1 were from *M. truncatula* IMGAG version MT3.0 (http://www.medicago.org/genome/downloads/Mt3/).

(B) Purified recombinant MaT4, MaT5, and MaT6 malonyltransferase proteins separated by SDS-PAGE. The enzymes were expressed *in E. coli* as His-tagged fusions (~48 kD) and purified with nickel resin.

(C) to **(H)** Analysis of MaT4 activity.

(C) and **(F)** HPLC chromatographs showing substrates and products of malonyltransferase reactions catalyzed by recombinant MaT4 with A7G or K7G as substrate. Apigenin 7-*O*-glucoside malonate (A7GM) and kaempferol 7-*O*-glucoside malonate (K7GM) are indicated as products.

(D) and **(G)** Mass spectra for A7G and K7G, respectively.

(E) and **(H)** Mass spectra for the malonylated products A7GM and K7GM, respectively.

(I) to **(N)** Analysis of MaT5 activity.

(I) and **(L)** HPLC chromatographs showing substrates and products of malonyltransferase reactions catalyzed by recombinant MaT5 with Cy3G or P3G as substrate. Cyanidin 3-*O*-glucoside malonate (Cy3GM) and pelargonidin 3-*O*-glucoside malonate (P3GM) are indicated as products.

(J) and **(M)** Mass spectra for Cy3G and P3G, respectively.

(K) and **(N)** Mass spectra for the malonylated products Cy3GM and P3GM, respectively.

Note that the exact position of malonylation remains to be determined.

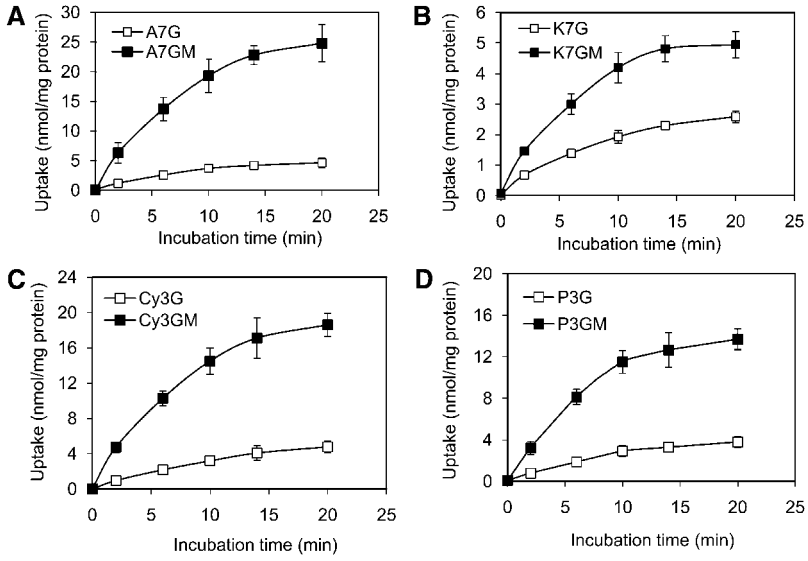

Figure 5. Preferential Uptake of Malonylated Flavonoid Glucosides by Yeast Microsomal Vesicles Containing MATE2.

(A) and **(B)** Time-dependent uptake of A7G and its malonylated product A7GM **(A)** or K7G and its product K7GM **(B)** into vacuolar vesicles prepared from yeast cells transformed with MATE2. Substrate concentration was 50 μM. Results are means and SD of three replicate uptake assays.

(C) and **(D)** Time-dependent uptake of Cy3G and Cy3GM **(C)** or P3G and P3GM **(D)** from malonylation reactions into membrane vesicles from yeast cells expressing MATE2. The substrate concentrations in reaction mixtures were as follows: Cy3G, ~95 μM; Cy3GM, ~65 μM; P3G, ~102 μM; P3GM, ~75 μM.

Results are means and SD of MATE2-mediated uptake, after subtracting vector controls, from three replicate uptake assays.

localization. Compared with optical sections of free GFP control (~20 sections), which show signals on both nucleus and many thick cytosolic bundles in tobacco epidermal cells (Figure 6G), GFP-MaT4 was observed to be cytosolic, exhibiting no signal inside the nucleus but only around the nuclear membrane and thick cytosolic bundles (Figure 6H), whereas GFP-MaT5 appeared to exhibit both endoplasmic reticulum (ER) and cytosolic localization (Figure 6I). GFP-MaT6 was evenly distributed in the thin ER network as well as around the nuclear membrane (Figure 6J).

To further confirm the subcellular localization of the malonyltransferases, total protein extracts from tobacco leaves expressing free GFP and the three GFP-MaT fusions were fractionated into soluble and microsomal membrane fractions, which were then analyzed on protein gel blots probed with anti-GFP antibody and an antibody against BiP, an ER marker. Free GFP and GFP-MaT4 were recovered in the soluble fraction, whereas GFP-MaT5 was detected in both soluble and microsomal fractions, and GFP-MaT6 was mainly in the microsomal fraction (see Supplemental Figure 15 online).

Loss of MATE2 Expression Changes Leaf Pigmentation, Flower Color, and (Malonylated) Flavonoid Profiles

To address the physiological function of MATE2 in *Medicago*, *Tnt1* retrotransposon insertion mutants that abolished *MATE2* expression were isolated from the *Medicago Tnt1* insertion population established at the Noble Foundation (Tadege et al., 2008). By PCR screening of *Tnt1* population DNA pools with both *Tnt1* left and right border primers and *MATE2* gene-specific primers (see Supplemental Table 2 online), as well as searching the flanking sequence tag collection from the population (http://bioinfo4.noble.org/mutant/database.php) with the *MATE2* genomic sequence, we obtained four lines with independent *Tnt1* insertions in the *MATE2* gene (Figure 7A). Apart from *mate2-1*, with a *Tnt1* insertion in the first exon, the insertion sites in *MATE2* were all in introns; however, *MATE2* transcripts were effectively abolished in all homozygous lines (Figure 7B).

Under normal growth conditions, homozygous *mate2* mutant lines did not show altered vegetative growth or morphological phenotypes. However, the characteristic purple pigmentation in the trifoliate leaves of 1- to 2-week-old *M. truncatula* wild-type R108 was strongly reduced or even disappeared in *mate2* mutant lines (Figure 7C), and this effect was most apparent when viewing cross sections of leaves of *mate2* mutants compared with the wild type, especially leaves from which the epidermis had been stripped (Figure 7D; see Supplemental Figure 16 online). Quantification of anthocyanins from *mate2* and wild-type R108 plants showed that total anthocyanin levels decreased by more than 50% in mutants as compared with the wild type (Figure 7E). All four *mate2* mutant lines had paler flowers than wild- type R108 plants (Figure 7F). However, RT-PCR indicated that anthocyanin biosynthetic genes were still expressed in the *mate2* mutants (see Supplemental Figure 17 online). The decreased yellow pigmentation in *mate2* mutant lines may result from reduced accumulation of flavonoids in flower petals, since *MATE2* is strongly expressed in epidermal cells and vascular bundles in flowers. Flavonoid metabolites were therefore profiled in the mutants and corresponding null segregant controls. In *M. truncatula* leaves, apigenin, genistein, kaempferol, and quercetin represent more than

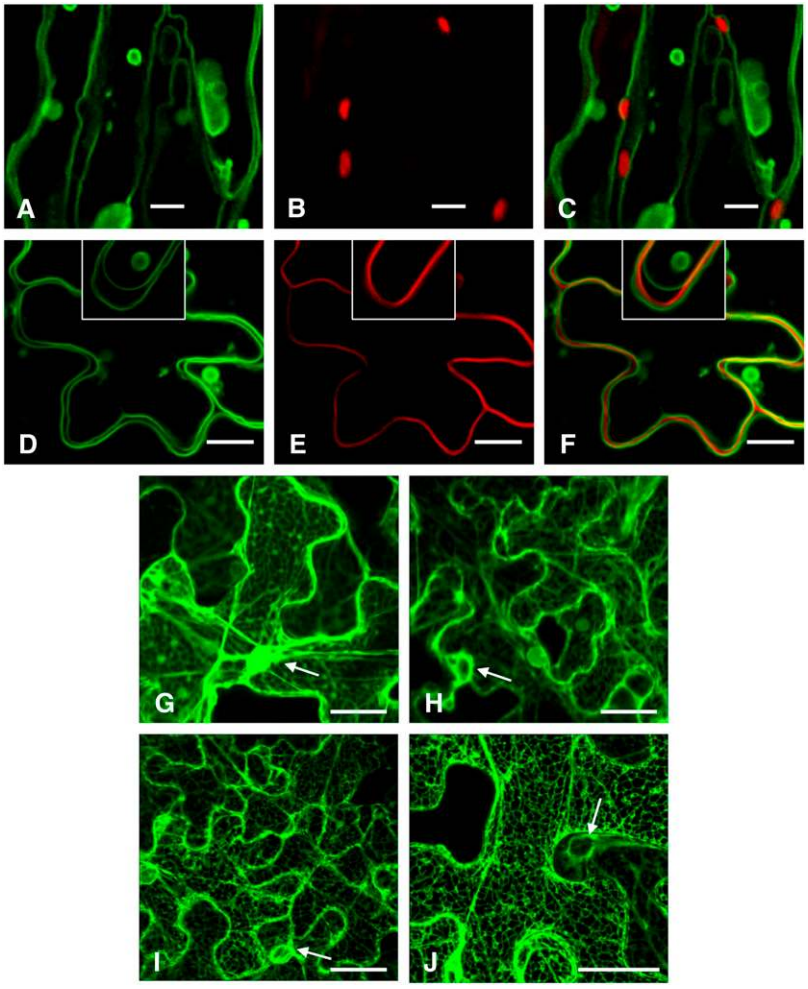

Figure 6. Subcellular Localization of MATE2, MaT4, MaT5, and MaT6.

MATE2-GFP, GFP-MaT4, GFP-MaT5, and GFP-MaT6 were driven by the cauliflower mosaic virus 35S promoter and transiently expressed in tobacco leaf epidermal cells. Stable expression of MATE2-GFP in *Arabidopsis* was made by *Agrobacterium*-mediated transformation. Materials were viewed by confocal microscopy.

(A) to **(C)** Fluorescence images of *Arabidopsis* petiole cells expressing MATE2-GFP. Bars = 25 μm.

(A) GFP fluorescence image.

(B) Chloroplast autofluorescence image.

(C) Merged GFP image and chloroplast autofluorescence image.

(D) to **(F)** Fluorescence images of *Arabidopsis* petiole cells expressing MATE2-GFP and stained with the dye FM4-64. Insets show enlarged images. Bars = 25 μm.

(D) GFP fluorescence image.

(E) FM4-64–labeled plasma membrane.

(F) Merged image of **(D)** and **(E)**.

(G) to **(J)** Fluorescence images of tobacco leaf epidermal cells expressing free GFP, GFP-MaT4, GFP-MaT5, or GFP-MaT6. Arrows show the nucleus. The image shows 20 Z-series sections combined (5 μm thickness). Bars = 25 μm.

(G) Fluorescence image of free GFP.

(H) Fluorescence image of GFP-MaT4.

(I) Fluorescence image of GFP-MaT5.

(J) Fluorescence image of GFP-MaT6.

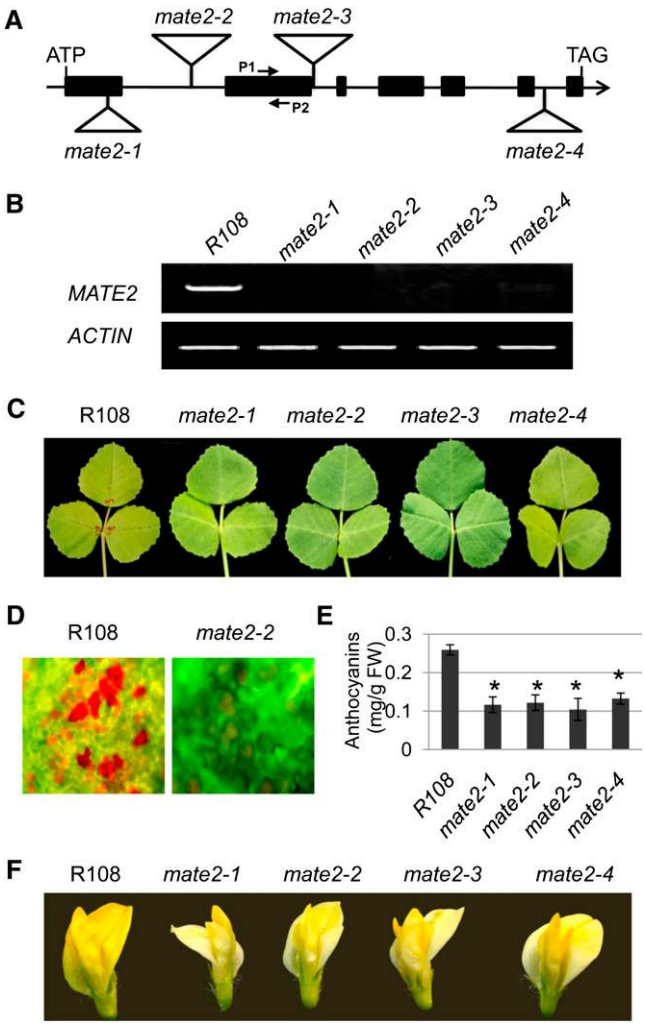

Figure 7. Loss-of-Function Analysis of *MATE2* in *M. truncatula*.

(A) The *MATE2* gene and the positions of the *Tnt1* retrotransposon insertions in *mate2-1*, *mate2-2*, *mate2-3*, and *mate2-4*. Introns (lines) and exons (black boxes) are shown. Positions of primers P1 and P2 designed for quantitative RT-PCR in the second exon are shown.

(B) RT-PCR analysis of *MATE2* transcripts in wild-type R108 and *mate2* mutants. *ACTIN* was used as an internal control. Primers used here are to amplify full-length MATE2 cDNA.

(C) Leaf pigmentation phenotypes of wild-type *M. truncatula* R108 and *mate2* mutant lines (4 weeks old).

(D) Anthocyanin pigments in leaf mesophyll cells of the *mate2* mutant and wild-type *M. truncatula* R108 (4 weeks old).

(E) Anthocyanin levels in 2-week-old seedlings of *mate2* mutants and wild-type R108. Values are means and SD from three biological replicates. Asterisks indicate that the flavonoid levels in *mate2* mutants are statistically different ($P < 0.05$, two-paired *t* test) from those in the corresponding wild-type plants. FW, fresh weight.

(F) Flower color phenotypes of wild-type *M. truncatula* R108 and *mate2* mutant lines 2 d post opening of petals.

30% of total flavonoids, and luteolin and kaempferol glycosides are the major flavonoid glycosides. All *mate2* mutants showed generally decreased flavonoid glycoside levels in both leaves and flowers (Figure 8A; see Supplemental Figure 18 online). Levels of Cy3G and luteolin 7-*O*-glucoside in both leaves and flowers decreased in *mate2* mutants compared with controls; in particular, K7G and kaempferol 3-*O*-rhamnoside contents were drastically reduced. However, A7G, naringenin 7-*O*-glucoside, biochanin A 7-*O*-glucoside, and formononetin 7-*O*-glucoside levels appeared to be increased in *mate2* mutants compared with controls. Levels of minor anthocyanins, such as D3G, P3G, D35G, and pelargonidin 3,5-di-*O*-glucoside (P35G), were also reduced in *mate2* leaves, but less so in flowers. Levels of flavonoid aglycones were also reduced in the *mate2* mutants, suggesting either feedback into the biosynthetic pathway or turnover of incorrectly stored products.

Because malonylated flavonoid glycosides were the preferred substrates for MATE2 in vitro, and these compounds, although abundant in roots and cell suspension cultures of *M. truncatula* (Farag et al., 2008), have not been described from the aerial portions of the plant, it was important to demonstrate their relative levels in wild-type and *mate2* plants. Both flower and leaf tissues contained the flavonoid glucoside malonates that were identified as MaT4 and MaT5 enzymatic products. However, the levels of these various flavonoid malonates in these tissues varied greatly over a wide range: L7G malonate, K7G malonate, G7G malonate, and A7G malonate were present at relatively high levels, whereas levels of Cy3G malonate and biochanin A 7-*O*-glucoside malonate were lower (Figure 8A). Loss of *MATE2* expression altered these flavonoid malonate profiles as compared with wild-type controls. Most flavonoid malonates, including L7G, naringenin 7-*O*-glucoside, A7G, and Cy3G malonates, accumulated to higher levels in *mate2* mutants than in wild-type plants (differences statistically significant at $P < 0.05$; Figure 8A). Whereas K7G malonate levels were reduced in a similar manner to K7G levels in *mate2* mutants, levels of G7G malonate showed no change. Changes in flavonoid malonate levels were also dependent on tissue type; for example, the levels of Cy3G malonate increased in *mate2* leaf tissues but not in flower tissues, whereas formononetin 7-*O*-glucoside malonate levels were reduced in *mate2* flower tissues but not in leaf tissues (Figure 8A).

Loss of Function of MATE2 Affects PA Biosynthesis in Seeds

E3′G levels were higher in *mate2* mutant flowers than in wild-type control flowers, suggesting that blocking the transport of anthocyanins into the vacuole may feed back to direct more anthocyanidin precursor flux into the PA biosynthesis pathway, leading to more E3′G production (Figure 8A). To further confirm that PA or PA precursor biosynthesis can indeed be enhanced by blocking anthocyanin transport, PA contents of seeds of *mate2* mutants and wild-type controls were determined. Four *mate2* mutant alleles all showed increased contents of both soluble and insoluble PAs in their seeds compared with those in their corresponding null segregant controls (Figure 8B). The increases in the *mate2-1*, *mate2-2*, and *mate2-3* lines were significant ($P < 0.01$–0.05), but the increase in *mate2-4* was not. Consistent with increased PA accumulation, decreased anthocyanin levels were also observed in the *mate2* lines (see Supplemental Figure 19 online).

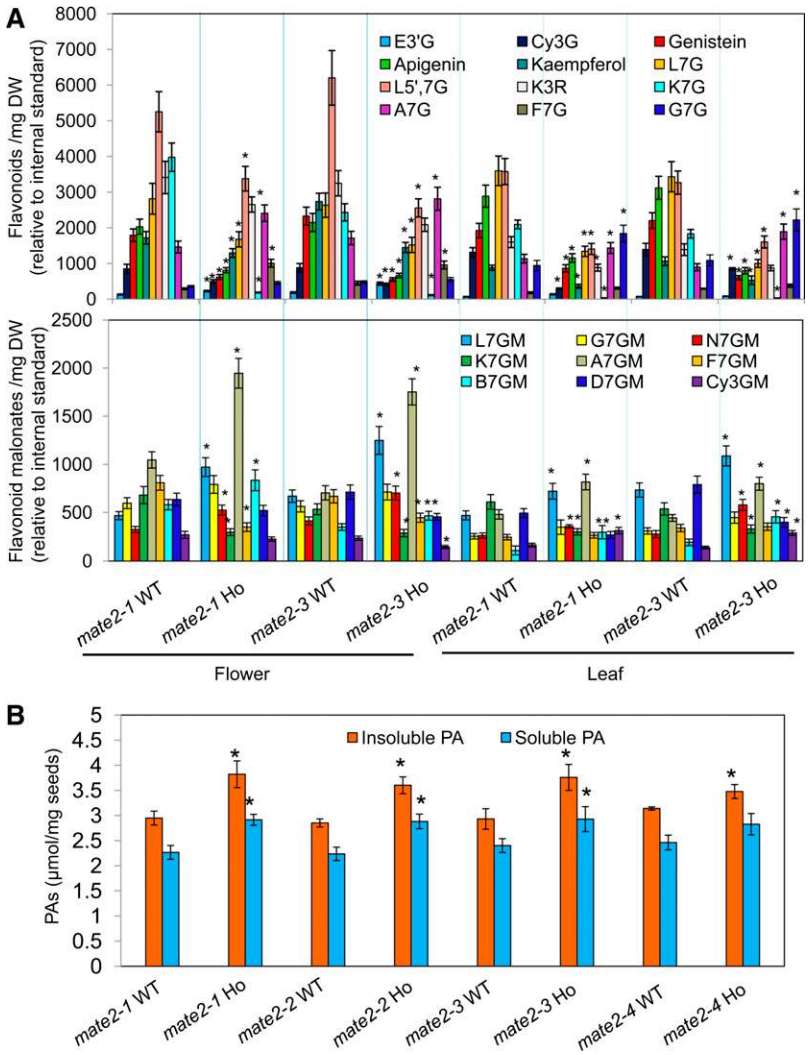

Figure 8. Flavonoid Profiles in *M. truncatula mate2* Mutants and their Null Segregant Controls.

Leaves from 4-week old seedlings and flowers 2 to 3 d post flowering were harvested from *mate2* mutants and wild-type plants for metabolite analysis by UPLC-ESI-TOF-MS. Mature seeds of *mate2* (*mate2* Ho) and null segregant controls (*mate2* WT) were analyzed for PA levels. Data are means and SD from three biological replicates. Asterisks indicate that the flavonoid levels in *mate2* mutants are statistically different ($P < 0.05$, Student's *t* test) from those in the corresponding wild-type plants.

(A) Top, profiles of flavonoids in *mate2* mutants and null segregant controls; bottom, profiles of flavonoid malonates in *mate2* mutants and null segregant controls. DW, dry weight.

(B) Contents of soluble and insoluble PAs in *mate2* mutants and null segregant controls.

DISCUSSION

Substrate Preferences for Flavonoid Transport

Our understanding of the subcellular distribution, transport, and storage of flavonoids is still in its infancy (Grotewold, 2004, Yazaki, 2005; Zhao and Dixon, 2010). This lack of knowledge limits our understanding of most cellular and subcellular processes involving flavonoids, the physiological roles of these compounds in plants, and our ability to engineer flavonoid accumulation for the improvement of agronomic traits or nutritional value.

The central vacuole plays a critical role in the accumulation of different flavonoids, including anthocyanins, (iso)flavones, and flavan 3-ol-derived PAs (Kitamura et al., 2004; Dixon et al., 2005). Dysfunction of the vacuole or loss of function of vacuolar flavonoid transporters can reduce flavonoid accumulation (Marinova et al., 2007a, 2007b). The ABC transporter MRP3 and a few MATE transporters (AM1 and AM3) have been suggested to transport anthocyanins into the vacuole (Goodman et al., 2004; Gomez et al., 2009). However, in none of these cases has a complete data set documenting transport properties, preferred substrates, cellular and subcellular localization, and genetic dissection been presented; all these aspects are

essential for a full understanding of flavonoid transporter function. Furthermore, the relationship between flavonoid modification and transport is still unclear, in particular whether the acyl modifications commonly found with anthocyanins and (iso)flavonoids are essential for transport and/or stabilization of the parent compounds once localized to the vacuole (Matern et al., 1983; Suzuki et al., 2002; Luo et al., 2007; Zhao and Dixon, 2010). This study, therefore, was undertaken to provide a complete description and dissection of flavonoid transport and modification in a genetically tractable system.

MATE2 Is a Vacuolar Flavonoid Transporter

MATE2 is phylogenetically related to the known flavonoid transporters MATE1, TT12, AM1, and AM3, all of which appear to be localized to the vacuolar membrane on the basis of GFP fusion imaging (Marinova et al., 2007a; Gomez et al., 2009; Zhao and Dixon, 2009). Using the same approach, MATE2-GFP also appears to be targeted to the vacuolar membrane in plant cells (tobacco, *Arabidopsis*, and onion epidermal cells) as well as in yeast cells. It is always a challenge to clearly distinguish the tonoplast from the plasma membrane in mature and highly vacuolated epidermal cells. However, by comparing MATE2-GFP signal with red chloroplast autofluorescence and plasma membrane labeling with FM4-64, we were able to conclude that MATE2-GFP is indeed a vacuolar membrane protein. Based on proteomic analysis, another MATE transporter, EET, was shown to be present on the tonoplast in *Arabidopsis* (Jaquinod et al., 2007).

MATE2 localization in yeast cells was confirmed both with MATE2-GFP imaging under confocal microscopy and by cofractionation of MATE2-GFP with vacuolar membranes following sucrose-density gradient centrifugation. MATE2 expressed in yeast not only transports several anthocyanin glucosides but also transports other flavonoid glucosides into vacuolar vesicles at a low efficiency.

MATE2 Preferentially Transports Malonylated Flavonoids

Many MATE transporters, such as DTX1 from *Arabidopsis* (Li et al., 2002), show a relatively broad substrate specificity. This is also the case for MATE2. In contrast to MATE1, which transports E3′G at a high efficiency and Cy3G at a lower efficiency but shows almost no transport activity toward other flavonoid glucosides, MATE2 transports various anthocyanidin glucosides with different hydroxylation patterns, flavonol glucosides, and flavone glucosides at lower efficiencies. However, MATE2 shows little transport activity toward E3′G and has a very different tissue-specific expression pattern from that of MATE1, indicating that the two transporters clearly possess different physiological functions.

Malonylated flavonoids are more efficiently transported by MATE2 than are their nonacylated precursors. Malonylation of flavonoid glucosides by MaT4, MaT5, or MaT6 increases not only their affinity for MATE2 but also their transport efficiency, as indicated by increased V_{max} values. Similar to other flavonoid transporters (Marinova et al., 2007a; Gomez et al., 2009; Zhao and Dixon, 2009), MATE2 shows almost no transport activity toward flavonoid aglycones. Therefore, MATE2 specially transports glycosyl- and malonyl-glycosyl–modified flavonoids, compounds that are widely present in *M. truncatula* (Farag et al., 2008; this work).

The nature of the forms in which flavonoids are preferentially transported has been actively discussed for many years (Zhao and Dixon, 2010). The anthocyanins that accumulate in the vacuoles of different plants are largely present in acylated forms (Matern et al., 1983; Markham et al., 2000; Zhang et al., 2006), and biochemical analysis suggests that the grapevine MATE transporters AM1 and AM3 specifically transport *p*-coumaroyl–acylated anthocyanidin glucosides (Gomez et al., 2009). Two major types of acylation, aromatic acylation (such as *p*-coumaroyl group addition) and aliphatic acylation (such as malonyl group addition), may have different physiological functions (Strack and Wray, 1994). It has been suggested that aromatic acylation enhances the color of anthocyanins, whereas aliphatic acylation (usually malonylation) may stabilize flavonoids and increase the resistance of flavonoid glucoside malonates to enzymatic degradation (Suzuki et al., 2002; Luo et al., 2007). For example, the levels of (iso)flavone glucoside malonates in *M. truncatula* suspension cultures show much less change after elicitation of cells with yeast extract than do the levels of isoflavone glucosides inside the cells and corresponding aglycones in the culture medium (Farag et al., 2008), suggesting that the flavonoid glucoside malonates are a stable storage form.

Malonylation of flavonoids occurs widely in plants, and malonyltransferases have been characterized from several different species (Suzuki et al., 2002, 2003, 2004; Luo et al., 2007; Yu et al., 2008). An NMR study showed that malonylation, but not *p*-coumaroylation, of flavonoids induces a conformational change that might facilitate their transport and storage in the vacuole (Matern et al., 1983), possibly through improved solubility and reaction with other vacuolar components (Matern et al., 1983; Markham et al., 2000; Zhang et al., 2006). However, the precise physiological function of flavonoid malonylation has yet to be defined (Boller and Wiemken, 1986; Springob et al., 2003; Luo et al., 2007; Yu et al., 2008). A role for malonylation in targeting compounds for vacuolar transport as opposed to extracellular secretion is supported by the recent demonstration that malonylation of xenobiotic phenolic glucosides leads to their preferential transport to the vacuole in *Arabidopsis* (Taguchi et al., 2010).

This study demonstrates that malonylation of anthocyanins or other flavonoids facilitates their transport into the vacuole by a defined transporter and shows that MaT4, localized to the cytoplasm, MaT5, localized to the ER, and MaT6, localized to both the cytoplasm and ER, are likely important for flavonoid modification and therefore transport. The fact that the malonyl group addition to the sugar moiety of flavonoid glucosides increases their affinity for, and transport efficiency by, the MATE2 transporter effectively links cytosolic flavonoid modifications to transport and storage in the vacuole. This link could be further addressed upon the availability of *Tnt1* insertion mutants in the malonyltransferase genes.

Mechanisms in addition to acylation have been also suggested to facilitate anthocyanin transport. Although genetic evidence indicates that the maize ABC transporter MRP3 is involved in

vacuolar transport of anthocyanins (Goodman et al., 2004), and Marrs et al. (1995) showed that Cy3G conjugated with glutathione by glutathione *S*-transferase (GST) was recognized as a substrate for transport into vacuoles by the GS-X pump in maize, it is now believed that MRP3 and other related transporters are unlikely to transport glutathionylated anthocyanins (Kitamura, 2006). This is because such compounds have yet to be identified in plants, and the GST activity of TT19, a GST required for PA accumulation in *Arabidopsis*, is not required for its function (Mueller et al., 2000).

Coregulation of MATE2 with Flavonoid Biosynthesis and Modification Genes

Flavonoid biosynthetic genes are usually coordinately regulated by developmental and environmental cues such as growth stage (in culture) and light (Lepiniec et al., 2006). Furthermore, metabolic channeling has been proposed for flavonoid biosynthetic enzymes (Winkel, 2004; Jørgensen et al., 2005), suggesting the need for tight coregulation of protein amounts. Tissue-specific coregulation of core flavonoid biosynthetic genes, glycosyltransferases, malonyltransferases, and MATE2 are evident from analysis of microarray databases and our experiments. UGT78G1 is a glycosyltransferase that shows activity toward anthocyanins and a range of other flavonoids in vitro and is, along with MATE2 and *MaT4*, controlled in *Medicago* by the anthocyanin-regulatory MYB transcription factor LAP1 (Modolo et al., 2007; Peel et al., 2009). Genetic evidence indicates that the major function of UGT78G1 in vivo is the 3-*O*-glycosylation of anthocyanidins (Peel et al., 2009). The anthocyanin malonyltransferase gene *MaT5* is primarily expressed in flowers and roots, while *MaT6* is primarily expressed in leaf, stem, and flowers. Since MaT5 and MaT6 showed very similar substrate specificities, it is probable that *M. truncatula* utilizes these two genes in different tissues for similar functions.

Physiological Function of MATE2

Flavonoid pigments, including flavonols, flavones, and anthocyanins, can interact with each other for copigmentation and aggregation within the vacuole or be selectively compartmentalized, as in petal cells; these fates can influence color hue, intensity, and stability (Markham et al., 2000). The abundant flavonols and flavones, as well as their complexes with proteins or lipids, often contribute to the yellow petal color (Markham et al., 2000). Similar to mutants affecting other flavonoid transporters such as MRP3, TT12, and MATE1 (Goodman et al., 2004; Marinova et al., 2007a; Zhao and Dixon, 2010), *mate2* mutant alleles display reduced leaf pigmentation and pale flower color, as compared with wild-type *M. truncatula* plants, which exhibit purple anthocyanin pigmentation in the trifoliate leaves and brownish yellow flowers. Metabolite profiling data suggest that the leaf pigmentation and flower color phenotypes in *mate2* mutants may be attributable to the decreased levels of anthocyanins and other flavonoid compounds in leaf and floral tissues. These data indicate that MATE2 plays an important role in flavonoid accumulation in *Medicago*, and the differentially altered levels of upstream intermediates, an array of flavonoid glucosides and aglycones, in the *mate2* mutants suggests that MATE2 activity exerts positive feedback on upstream metabolism. Mutation of the MATE transporter FFT (At4g25640) in *Arabidopsis* results in a decrease in levels of flavonol glucosides, but not anthocyanins; this study did not determine levels of malonylated flavonoids or in vitro transport properties (Thompson et al., 2010). It appears that FFT has a somewhat different transport function from MATE2.

It is interesting that the levels of some flavonoid glycoside malonates are increased in *mate2* mutants, whereas others are reduced. Seeds of the *Arabidopsis tt12* mutant accumulate epicatechin glucoside, as this is the preferred substrate for the TT2 MATE transporter (Zhao and Dixon, 2009; Kitamura et al., 2010), and is probably further metabolized to PAs following transport to the vacuole. The further metabolic fates of flavonoid malonyl glycosides are poorly understood, as are their potential stabilities compared with the unmodified glycoside if they are allowed to accumulate in the cytoplasm due to blockage of vacuolar transport.

The presence of MATE2 transcripts in vascular bundles of both leaf and petal suggests that MATE2 might also be associated with long-distance transport of flavonoids, but the mechanisms underlying such transport of flavonoids between shoots and roots remain to be determined (Buer et al., 2007).

Competition between Anthocyanin and PA Biosynthesis

Several pieces of evidence suggest competition between anthocyanin and PA biosynthesis, but the mechanisms remain unclear (Lee et al., 2005; Marinova et al., 2007a). MATE1 is specifically expressed in the seed coat where PAs accumulate in *M. truncatula* (Zhao and Dixon, 2009). MATE2 is also expressed in developing seeds, but at low levels. While the levels of Cy3G are much lower in *mate2* flowers than in the wild type, E3′G levels, mainly from the coharvested young pods, are higher, suggesting that blocking MATE2-mediated transport of anthocyanins into the vacuole directs more anthocyanidin into PA biosynthesis. ANR expression in *mate2* mutants was not higher than in controls, suggesting that this effect is probably one of substrate availability. This phenomenon is also supported by the observation that *mate2* mutant seeds contain more soluble and insoluble PAs than controls. Blocking of anthocyanin transport may lead to temporary accumulation of Cy3GM and Cy3G and inhibition of modification enzyme activity, which then makes more cyanidin available for ANR to synthesize epicatechin, which is then converted to E3′G for vacuolar transport (by MATE1) and PA biosynthesis.

Alternative Transport Pathways for Anthocyanins

Although MATE2 efficiently transports glycosylated/malonylated anthocyanidins into the vacuole and functions in anthocyanin accumulation during leaf pigmentation and flavonoid accumulation in flowers, we cannot exclude the possibility of other mechanisms for flavonoid transport. Anthocyanin pigment–containing bodies have been observed moving in the cytoplasm of some plant cells, such as cultured maize and grapevine cells (Grotewold et al., 1998; Zhang et al., 2006). Membrane vesicle

trafficking–mediated transport of anthocyanins into the central vacuole has also been proposed (Grotewold, 2004; Poustka et al., 2007; Pourcel et al., 2010). However, such phenomena have only been observed in a limited number of plants (Grotewold, 2004). We have not observed anthocyanin bodies in *M. truncatula* leaf or flower petal cells. Furthermore, in *Medicago* plants producing massive amounts of anthocyanins as a result of constitutive expression of the *LAP1* transcription factor, several membrane transporters including *MATE2* are significantly up-regulated, whereas genes encoding known proteins involved in vesicle trafficking, such as SNAREs and GTPases, are not (Peel et al., 2009). Clearly, MATE2 represents one route for vacuolar transport of anthocyanins and other flavonoids in *Medicago*, but others cannot be ruled out, especially as the loss of function of *MATE2* does not result in a complete loss of flavonoid glycoside accumulation.

METHODS

Plant Materials and *Medicago truncatula Tnt1* Mutant Screening

Medicago truncatula plants were grown in the greenhouse as described previously (Zhao and Dixon, 2009). Reverse genetic screening of *M. truncatula Tnt1* mutants in the R108 background was performed as described previously (Peel et al., 2009). Two *MATE2 Tnt1* insertion mutant lines, NF5697 (*mate2-1*) and NF5176 (*mate2-2*), were identified through PCR-based screening of 10 superpools of pooled DNA samples from 5000 *Tnt1* insertional mutant lines of *M. truncatula* (Tadege et al., 2008) using a combination of *MATE2*- and *Tnt1*-specific primers (see Supplemental Table 2 online). The *Tnt1* insertion site in *MATE2* was verified by sequencing. Two other *Tnt1* lines, NF0737 and NF3103, were identified in silico through analysis of *Tnt1* flanking sequences in the mutant population (http://bioinfo4.noble.org/mutant/line2.php), and the *Tnt1* insertion sites were confirmed by PCR. Loss/reduction in *MATE2* transcripts in homozygous lines of these four independent *Tnt1* mutants was confirmed by RT-PCR.

Cloning and Vector Construction

The *MATE2*, *MaT4*, *MaT5*, and *MaT6* open reading frames (ORFs) were cloned from a cDNA library constructed from *M. truncatula* wild-type (R108) flower tissues (0–5 d post flowering) with forward and reverse primers that enabled PCR fragments to be directionally cloned into pENTR vector (see Supplemental Table 2 online). Total RNA was extracted from flowers of *M. truncatula* using the RNeasy plant mini kit procedure (Qiagen). First-strand cDNA was synthesized from total RNA with the SuperScript III First-Strand Synthesis system (Invitrogen) according to the manufacturer's protocol. The *MATE2* ORF was amplified with MATE2-5′ forward and MATE2-3′ reverse primers, and MaT4, -5, and -6 ORFs were cloned with corresponding forward and reverse primer pairs (see Supplemental Table 2 online). The PCR products were cloned into pENTR/D-TOPO vector (Invitrogen) for sequencing, and the confirmed clones were subcloned into Gateway destination vectors, the yeast expression vector pYESDEST52 (uracil selectable marker), His-tagged fusion protein expression vector pDEST17 for expression in *Escherichia coli*, or the plant binary vector pB2GW7 by recombination using Gateway LR Clonase (Invitrogen).

The MATE2-GFP fusion was constructed by cloning the *MATE2* ORF in frame with the N terminus of GFP. The *MATE2* ORF was amplified with the primers MATE2-GFP-5′ and MATE2-GFP-3′ (see Supplemental Table 2 online). PCR products were subcloned into the yeast GFP fusion cassette shuttle vector pHGDP-GFP (Zhao et al., 2009) in frame with the N terminus of GFP. The construct pHGDP-MATE2-GFP was transformed into yeast cells for checking MATE2-GFP expression. A 2.1-kb MATE2-GFP coding sequence was then amplified with the primer pair MATE2 SFI-5′ and MATE2 SFI-3′ (see Supplemental Table 2 online) and subcloned into pENTR/D-TOPO vector, followed by subcloning into the plant binary vector pB2GW7 (Invitrogen; Karimi et al., 2002) by recombination with Gateway LR Clonase. The 35S:MATE2-GFP construct was used for localization studies. All clones were confirmed by sequencing.

Chemicals and Reagents

Flavonoid aglycones, anthocyanidins, Cy3G, D3G, D35G, P3G, P35G, daidzein 7-*O*-glucoside, and other flavonoid glucosides were obtained from Indofine Chemical Company. Malonylated flavonoids were generated using MaT4 and MaT5 enzyme reactions in this study.

Yeast Culture, Transformation, and Preparation of Microsomal Fractions

Saccharomyces cerevisiae W303a (*Mat ade2-1 ura3-1 his3-11,15 trp1-1 leu2-3,112 can1-100*) was used to express MATE2. The Gateway yeast expression vectors pYESDEST52 (Invitrogen) and pYES harboring MATE2 were transformed into W303a by the polyethylene glycol/lithium acetate method (Zhao and Dixon, 2009). Yeast growth, induction of MATE2 expression by galactose, and microsomal preparation were conducted as described previously (Zhao and Dixon, 2009).

Transport Activity Assays

Flavonoid uptake by vacuolar membrane vesicles was performed at 25°C as described previously (Zhao and Dixon, 2009). Briefly, the 600- to 1000-μL assay mixtures contained 25 mM Tris-MES (pH 8.0), 0.4 M sorbitol, 50 mM KCl, 5 mM Mg-ATP, 0.1% (w/v) BSA, the indicated concentrations of transport substrate, and microsomal preparations (~300 μg of proteins). The flavonoids taken up into the membrane vesicles were extracted with 50% (v/v) methanol for 1 h on a shaker and analyzed by HPLC. Inhibitor assays were conducted with 1 mM vanadate, 5 mM gramicidin D, 0.1 mM bafilomycin A1, or 5 mM NH_4Cl in the reaction mixture for 8 min. Transport inhibitor stock solutions were 1 M vanadate in water, 5 mM bafilomycin A1 in DMSO, 5 mM gramicidin D in DMSO, and 1 M NH_4Cl in water. Corresponding solvent controls were included.

For competition assays with yeast membrane vesicles expressing MATE2, various concentrations of flavonoid glucosides were included in the uptake assay with 100 μM Cy3G as substrate. After incubation at 25°C for 10 min, transported flavonoids were extracted from vesicles as described (Zhao and Dixon, 2009) and measured by HPLC. Reverse-phase HPLC analyses were performed on an Agilent HP1100 HPLC apparatus using a gradient mobile phase, solvent A (1% phosphoric acid) and B (acetonitrile) at 1 mL/min flow rate: 0 to 5 min, 5% B; 5 to 10 min, 5 to 10% B; 10 to 25 min, 10 to 17% B; 25 to 30 min, 17 to 23% B; 30 to 65 min, 23 to 50% B; 65 to 79 min, 50 to 100% B; 79 to 80 min, 100 to 5% B. Data were collected at 206 and 530 nm for epicatechin and cyanidin derivatives, respectively. Identifications were based on chromatographic behavior and UV spectra compared with those of authentic standards.

Malonyltransferase Expression, Activity Assay, and Enzyme Product Identification

The full-length ORFs of *MaT4*, *MaT5*, and *MaT6* were cloned by PCR using their gene-specific primers (see Supplemental Table 2 online). PCR products were cloned into pENTR/D/TOPO TA vector (Invitrogen) for sequencing. Confirmed constructs were used for in vitro recombination

into destination vectors. For heterologous expression in *E. coli*, these genes were recombined with pDEST17 vector using Invitrogen Clonase LR. Confirmed pDEST-MaT4, pDEST-MaT5, and pDEST-MaT6 constructs were transformed into BL21 (DE3) cells for expression of proteins. Proteins were induced by 0.4 mM isopropyl-L-thio-β-D-galactopyranoside at 16°C overnight. After purification with a MagneHis protein purification system according to the manufacturer's instructions (Promega), malonyl transferase activity was assayed in reaction mixtures (100 μL) consisting of 20 mM potassium phosphate buffer (pH 7.0), 60 μM malonyl-CoA, 120 μM flavonoid glycoside, and enzyme (~0.5 μg of protein). The reaction was terminated by adding 200 μL of methanol after incubation at 30°C for 20 min. Enzymatic products in the reaction mixture were analyzed by reverse-phase HPLC as described previously (Zhao and Dixon, 2009). Malonylated flavonoid products from enzyme assays were identified by ESI-LC-MS. HPLC separation was achieved using a reverse-phase, C18 (5 μm, 4.6 × 250 mm) column (J.T. Baker) on an Agilent HP1100 HPLC apparatus using a step gradient mobile phase, solvent A (0.1% acetic acid) and B (acetonitrile) at 0.8 mL/min flow rate: 0 to 5 min, 5% B; 5 to 15 min, 5 to 15% B; 15 to 20 min, 15 to 17% B; 20 to 25 min, 17 to 23% B; 25 to 60 min, 23 to 50% B; 60 to 60.5 min, 50 to 95% B; 60.5 to 70.5 min, 95% B. All mass spectra were acquired using a Bruker Esquire LC apparatus equipped with an electrospray ionization source in the positive mode. Positive ion ESI was performed using a source voltage of 3000 V and capillary offset voltage of −70.7 V. Nebulization was achieved using nitrogen gas at a pressure of 70 p.s.i. Desolvation was aided by using a counter current gas of nitrogen at a pressure of 12 p.s.i. The capillary temperature was set at 350°C. Mass spectra were recorded over the range of 50 to 2200 m/z. The Bruker ion trap was operated under an ion current control of 20,000 with a maximum acquire time of 100 ms and a trap drive setting of 50.

Determination of Transport and Enzyme Kinetics

Transport assays were performed with different concentrations of Cy3G, D3G, D35G, P3G, P35G, and their malonylated derivatives (from 25 to 200 μM) and 5 mM Mg-ATP. After incubation at 25°C for 10 min, transported glycosides were measured by HPLC as described above. Kinetics of the malonyltransferases were determined with various flavonoid glycoside acceptors in 20-min incubations at 30°C. Lineweaver-Burk plots were used to calculate K_m and V_{max} values. Protein concentrations were determined using a Bio-Rad Protein Assay kit with BSA as the standard.

Localization of GFP Fusions by Confocal Microscopy

Five micrograms of plasmid DNA containing *35S:MATE2-GFP* or *35S:GFP* was mixed with 20 μL of an aqueous suspension containing 1.0-μm gold particles. After washing, the gold was spread onto plastic carrier discs for biolistic bombardment of tobacco (*Nicotiana tabacum*) and onion (*Allium cepa*) epidermal cells using a Bio-Rad 1000/HE particle delivery system. After 15 to 18 h, epidermal cells were viewed directly with a TCS-SP2 AOBS confocal laser scanning microscope (Leica Microsystems) to examine the localization patterns of MATE2-GFP. Alternatively, *Arabidopsis thaliana* (ecotype Columbia) was transformed with *Agrobacterium tumefaciens* AGl1 harboring the *35S:MATE2-GFP* construct by the floral dipping method (Clough and Bent, 1998). F1 seeds were selected on half-strength Murashige and Skoog plates containing appropriate antibiotics. Positive transgenic seedlings were used for imaging.

To compare the difference between MATE2-GFP–labeled tonoplast and plasma membrane, *Arabidopsis* leaf epidermal cells expressing MATE2-GFP were stained with a 10 μM aqueous solution of the dye FM4-64 for 10 min before being observed with the confocal microscope. FM4-64–labeled plasma membrane was excited at 543 nm with the argon laser, and emission was detected from 620 to 680 nm. Chloroplasts were visualized at 560 to 610 nm under excitation at 543 nm. All images were acquired at a resolution of 512 × 512 pixels using a 60×/1.20 water-immersion objective and analyzed with Leica LAS AF software or a Bio-Rad MRC 1024 ES confocal laser scanning microscope with Laser Sharp 2000 software for analysis.

Determination of the subcellular localizations of MaT4 and MaT5 was performed by tobacco leaf infiltration. pGFP-MaT4 and pGFP-MaT5 were transformed into *Agrobacterium* strain AGL1, and colonies were selected and grown at 28°C in a shaker in Luria-Bertani broth containing 100 μg/mL spectinomycin and 50 μg/mL ampicillin. Bacterial cells were pelleted and resuspended in infiltration medium (10 mM MES, pH 5.6, 10 mM $MgSO_4$, and 150 μM acetosyringone) at an OD_{600} of ~0.5. The bacteria were then infiltrated into the abaxial epidermal surface of a tobacco leaf with a syringe, and the plant was grown at room temperature for 2 to 3 d. A small piece of the infiltrated leaf tissue was then cut out and mounted in water for confocal microscopy. Imaging of GFP and GFP fusion proteins was performed using a Leica TCS SP2 inverted confocal microscope using a 63× water-immersion objective and Leica Confocal software. Serial optical sections of 0.5 μm were obtained at a resolution of 512 × 512 pixels using an excitation wavelength of 488 nm, and emissions were collected between 500 and 560 nm and analyzed by Leica LAS AF software.

In Situ Hybridization

In situ hybridization of *MATE2* transcripts in young leaves and flowers of *M. truncatula* R108 was conducted as described previously (Zhou et al., 2010). Leaves (3 weeks old) or flowers (0–3 d before flower opening) were sampled and fixed for hybridization with probes generated by PCR using the primers shown in Supplemental Table 2 online.

Quantitative RT-PCR

Total RNA was isolated from *M. truncatula* tissues using the RNeasy plant mini kit (Qiagen) for cDNA synthesis. Equal amounts of total RNA were treated with DNase I (Invitrogen) and were subsequently heat inactivated. cDNAs were synthesized with the SuperScript III First-Strand Synthesis system (Invitrogen). Diluted fractions were used for quantitative RT-PCR with an ABI PRISM 7900 HT sequence detection system (Applied Biosystems) as described previously (Zhao and Dixon, 2009). Quantitative RT-PCR data were analyzed using SDS 2.2.1 software (Applied Biosystems). PCR efficiency was estimated using the LinRegPCR software (Ramakers et al., 2003), and the transcript levels were determined by relative quantification (Pfaffl, 2001) using the *M. truncatula ACTIN* gene as a reference. For RT- PCR (Promega; Mix go polymerase), *Medicago MATE2* and *ACTIN* were amplified for 25 cycles (94°C for 30 s, 58°C for 30 s, and 72°C for 40 s) as described previously (Zhao and Dixon, 2009). Primers are shown in Supplemental Table 2 online.

Metabolite Profiling by UPLC-ESI-Quadrupole Time-of-Flight-MS

Leaf and flower tissue was ground into powder in liquid nitrogen and lyophilized. Dried tissues (~10.0 mg) were weighed into 1-g glass vials. Three biological replicates were extracted in 2 mL of 80% methanol containing 4 μg/mL puerarin (internal standard) for 2 h at room temperature with agitation. After centrifugation, the supernatants were analyzed with a Waters Acquit UPLC system fitted with a hybrid quadrupole time-of-flight (QTOF) Premier mass spectrometer (Waters). A reverse-phase, 1.7-μm UPLC BEH C18, 2.1 × 150 mm column (Waters) was used for separations. The mobile phase consisted of eluent A (0.1% [v/v] acetic acid/water) and eluent B (acetonitrile), and separations were achieved using a linear gradient of 95 to 30% A over 30 min, 30 to 5% A over 3 min, and 5 to 95% A over 3 min. The flow rate was 0.56 mL/min, and the

column temperature was maintained at 60°C. Masses of the eluted compounds were detected in the negative ESI mode from 50 to 2000 mass-to-charge ratio. The QTOF Premier mass spectrometer was operated under the following instrument parameters: desolvation temperature of 375°C; desolvation nitrogen gas flow of 850 liters/h; capillary voltage of 2.9 kV; cone voltage of 48 eV; and collision energy of 10 eV. The MS system was calibrated using sodium formate, and raffinose was used as the lockmass. Metabolites were identified based on accurate masses and retention times relative to authentic standards. Data Bridge (Mass Lynx version 4.1) was used to convert the raw data files to NetCDF. Relative abundances were calculated using MET-IDEA, and the peak areas were normalized by dividing each peak area by the value of the internal standard peak area.

The flavonoid glucoside malonates generated and identified by LC-ESI-MS/MS from MaT4-catalyzed flavonoid 7-*O*-glucoside and MaT5-catalyzed anthocyanin (Cy3G and P3G) malonylation reactions were run on UPLC-ESI-QTOF-MS under the above conditions. Using these flavonoid glucoside malonates and anthocyanin malonates as standards in our chemical library, the flavonoid malonates in *M. truncatula* tissues were identified by comparison of retention times, UV spectra, and mass spectra, and quantified relative to the same internal standard (puerarin).

Analysis of PAs and Anthocyanins

Soluble and insoluble PAs from mature *M. truncatula* seeds were measured as described previously (Zhao and Dixon, 2009). Epicatechin and proanthocyanidin B1 were used for making standard curves for the determination of soluble and insoluble PAs, respectively. The levels of anthocyanins in leaves and mature seeds were quantified as described previously (Pang et al., 2008) with cyanidin-3-*O* glucoside as the standard.

Protein Gel Blotting

Total protein extracts from yeast cells expressing MATE2-GFP or tobacco leaves expressing GFP-MaT4, GFP-MaT5, GFP-MaT6, or free GFP were subjected to fractionation by sucrose-density gradient centrifugation as described previously (Zhao and Dixon 2009). About 20 μg of proteins from the resulting fractions was loaded and run on precast 4 to 12% gradient SDS-PAGE gels (Nupage; Invitrogen) and transferred to nitrocellulose or polyvinylidene difluoride membranes. After electrophoresis and transfer to polyvinylidene difluoride membranes, proteins were blotted with anti-GFP (Invitrogen), anti-V-H^+-ATPase (Agrisera), anti-PM-H^+-ATPase (Agrisera), or anti-BiP (Agrisera) antibody raised in rabbits and then visualized by horseradish peroxidase–conjugated secondary antibody raised against rabbit IgG. Signals were visualized by enhanced chemiluminescence (ECL kit; Amersham).

Leaf Cross Sectioning

Discs from the bases of trifoliate leaflets of *M. truncatula* wild-type R108 and *mate2* mutants were excised and fixed in a specimen block. Leaf disc sections of 100 μm thickness were made using a vibratome (series 1500; Ted Pella). Sections were observed and photographs taken using a Nikon Microphot-FX system with a Nikon DXM 1200 color camera.

Clustering Analysis of Flavonoid Gene Expression Patterns

Clustering analysis used expression data obtained from the publicly available MtGEA version 2 (156 chips from 64 experiments; http://bioinfo.noble.org/gene-atlas/v2/). Expression data were transformed to $\log_2$, and hierarchical clustering was conducted using MEV software (http://www.tm4.org/mev/) based on Pearson correlation. Statistical verification of the probabilities for the roots was determined using Pvclust (Suzuki and Shimodaira, 2006).

Phylogenetic and Topological Analyses

Alignment of protein sequences was done with ClustalW (http://www.ebi.ac.uk/clustalw/). Formatting of aligned sequences was done with the box shade program (http://www.ch.embnet.org/software/BOX_form.html). Sequence alignments were analyzed with Mesquite software, and the nonrooted neighbor-joining tree was generated by PAUP 4.0 BETA programs. Topological analysis for transmembrane domains was performed using the TMHMM2 program in SMART (http://smart.embl-heidelberg.de).

Accession Numbers

Sequence data from this article can be found in the *Arabidopsis* Genome Initiative or GenBank/EMBL databases under the following accession numbers. *Medicago truncatula* MATE2, HM856605; MATE1, ACX37118; and predicted MATE transporter, AC122162_1.4. *Arabidopsis thaliana* MATE transporters TT12, NP_191462; FFT, BAE98568; FRD3, NP_001154595; ALF5, AAK21273; EDS5, AAL27003; and DXT1, NP_178496. *Solanum lycopersicum* (tomato) MTP77, AAQ55183. *Nicotiana tabacum* (tobacco) JAT1, CAQ51477; Nt MATE1, BAF47751; Nt MATE2, BAF47752. *Hordeum vulgare* (barley) Hv ACCT1, BAF75822. *Vitis vinifera* MATE transporters AM1 and AM3, XP_002282932 and CAO69962, respectively. *Populus trichocarpa* predicted MATE transporter XP_002307572. *Ricinus communis* predicted MATE transporters XP_002532702 and EEF49069. *Brassica rapa* predicted MATE transporter, ACJ36213. *Sorghum bicolor* (sorghum) MATE transporter Sb MATE1, ABS89149. Flavonoid malonyltransferases from *M. truncatula* MaT1 (ABY91220), MaT2 (ABY91222), MaT3 (ABY91221), MaT4 (HM856606), MaT5 (HM856607), MaT6 (HM856608); *Salvia splendens* Ss 5MaT1 (AAR26386), Ss 3AT (AAR28757), and Ss 5MaT2 (AAL50566); *Dendranthema* × *morifolium* Dm 3MaT1 (AAQ63615) and Dm 3MaT2 (AAQ63616); *Senecio cruentus* Sc 3MaT (AAO38058); *Dahlia variabilis* Dv 3MaT (AAO12206); *Perilla frutescens* Pf 5MaT (AAL50565) and Pf 3AT (BAA93475); *Glandularia* × *hybrid* Gh 3MaT (AAS77402); *Lamium purpureum* Lp 3MaT (AAS77404); and *Gentiana triflora* Gt 5AT (BAA74428).

Supplemental Data

The following materials are available in the online version of this article.

Supplemental Figure 1. Amino Acid Alignments of MATE2 with MATE Transporters from Other Plant Species.

Supplemental Figure 2. Uptake of Cy3G by MATE2.

Supplemental Figure 3. Microarray and Quantitative RT-PCR Analysis of Tissue-Level Expression of Flavonoid Biosynthetic, Modification, and Transporter Genes in Wild-Type *M. truncatula* R108.

Supplemental Figure 4. Heat Map Mosaic Representation of Pearson Correlation Values between Each Gene in Figure 3A.

Supplemental Figure 5. Amino Acid Alignments of Conserved Motifs in MaT4, MaT5, and MaT6 from *M. truncatula* with Other Plant Malonyltransferases.

Supplemental Figure 6. HPLC Analysis of MaT4 Malonyltransferase Activity toward Various Flavonoid Glucosides.

Supplemental Figure 7. HPLC Analysis of Anthocyanin Malonyltransferase Reactions Catalyzed by MaT5 or MaT6.

Supplemental Figure 8. ESI-LC-MS Analysis and Identification of Flavonoid Glucoside Malonates from MaT4 Malonyltransferase Enzyme Assays.

Supplemental Figure 9. Schematic of MaT4-, MaT5-, and MaT6-Catalyzed Malonylation of Flavonols, Flavones, Isoflavones, and Anthocyanins.

Supplemental Figure 10. Concentration-Dependent Uptake of Pelargonidin and Delphinidin Monoglucosides and Diglucosides by MATE2.

Supplemental Figure 11. Concentration-Dependent Uptake of Flavones and Flavonol (Malonyl)Glucosides by MATE2.

Supplemental Figure 12. Topological Analysis of MATE2 and Related MATE Transporters from Other Plant Species.

Supplemental Figure 13. Localization and Transport Activity of MATE2-GFP Expressed in Yeast.

Supplemental Figure 14. Localization of MATE2-GFP Expressed in Tobacco and Onion Cells.

Supplemental Figure 15. Protein Gel Blot Analysis of the Subcellular Localization of MaT4, MaT5, and MaT6 in Tobacco Plants.

Supplemental Figure 16. *M. truncatula* Leaf Pigmentation and Leaf Cross Sections of *mate2* Mutant and Wild-Type R108.

Supplemental Figure 17. Transcript Analysis of Flavonoid Pathway Genes in Wild-Type R108 and *mate2* Mutants.

Supplemental Figure 18. Flavonoid Profiles of *M. truncatula mate2* Mutants and their Null Segregant Controls.

Supplemental Figure 19. Anthocyanin Levels in Seeds of Mature *mate2* Mutant and Null Segregant Controls.

Supplemental Table 1. Kinetic Parameters of MaT4 and MaT5 Malonyltransferases from *M. truncatula* toward Various Flavonoid Glucosides.

Supplemental Table 2. Primers Used in This Study.

Supplemental Data Set 1. Alignment Corresponding to the Phylogenetic Analysis in Figure 2A.

Supplemental Data Set 2. Alignment Corresponding to the Phylogenetic Analysis in Figure 4A.

ACKNOWLEDGMENTS

We thank Xiaofei Cheng and Jiangqi Wen for screening transposon insertion lines, Junying Ma for assistance with in situ hybridization, Elison Blancaflor for help with cellular imaging, Carla Welch for assistance with plant growth, Scott McNeill and Broderick Stearns for assistance with photography, Darla Boydston for assistance with figure preparation, and Michael Udvardi and Rujin Chen for critical reading of the manuscript. The *M. truncatula* plants utilized in this research project, which are jointly owned by the Centre National de la Recherche Scientifique, were created through research funded, in part, by Grant 703285 from the National Science Foundation. This work was supported by Forage Genetics International and the Samuel Roberts Noble Foundation.

Received October 26, 2010; revised March 17, 2011; accepted March 22, 2011; published April 5, 2011.

REFERENCES

Ariga, T., Asao, Y., Sugimoto, H., and Yokotuska, T. (1981). Occurrence of astringent oligomeric proanthocyanidins in legume seeds. Agric. Biol. Chem. **45:** 2705–2708.

Bartholomew, D.M., Van Dyk, D.E., Lau, S.M., O'Keefe, D.P., Rea, P.A., and Viitanen, P.V. (2002). Alternate energy-dependent pathways for the vacuolar uptake of glucose and glutathione conjugates. Plant Physiol. **130:** 1562–1572.

Benedito, V.A., et al. (2008). A gene expression atlas of the model legume *Medicago truncatula*. Plant J. **55:** 504–513.

Boller, T., and Wiemken, A. (1986). Dynamics of vacuolar compartmentation. Annu. Rev. Plant Physiol. **37:** 137–164.

Buer, C.S., Muday, G.K., and Djordjevic, M.A. (2007). Flavonoids are differentially taken up and transported long distances in Arabidopsis. Plant Physiol. **145:** 478–490.

Clough, S.J., and Bent, A.F. (1998). Floral dip: A simplified method for *Agrobacterium*-mediated transformation of *Arabidopsis thaliana*. Plant J. **16:** 735–743.

Diener, A.C., Gaxiola, R.A., and Fink, G.R. (2001). *Arabidopsis ALF5*, a multidrug efflux transporter gene family member, confers resistance to toxins. Plant Cell **13:** 1625–1638.

Dixon, R.A., Xie, D.Y., and Sharma, S.B. (2005). Proanthocyanidins—A final frontier in flavonoid research? New Phytol. **165:** 9–28.

Dröse, S., and Altendorf, K. (1997). Bafilomycins and concanamycins as inhibitors of V-ATPases and P-ATPases. J. Exp. Biol. **200:** 1–8.

Durrett, T.P., Gassmann, W., and Rogers, E.E. (2007). The FRD3-mediated efflux of citrate into the root vasculature is necessary for efficient iron translocation. Plant Physiol. **144:** 197–205.

Farag, M.A., Huhman, D.V., Dixon, R.A., and Sumner, L.W. (2008). Metabolomics reveals novel pathways and differential mechanistic and elicitor-specific responses in phenylpropanoid and isoflavonoid biosynthesis in *Medicago truncatula* cell cultures. Plant Physiol. **146:** 387–402.

Frangne, N., Eggmann, T., Koblischke, C., Weissenböck, G., Martinoia, E., and Klein, M. (2002). Flavone glucoside uptake into barley mesophyll and Arabidopsis cell culture vacuoles. Energization occurs by H^+-antiport and ATP-binding cassette-type mechanisms. Plant Physiol. **128:** 726–733.

Furukawa, J., Yamaji, N., Wang, H., Mitani, N., Murata, Y., Sato, K., Katsuhara, M., Takeda, K., and Ma, J.F. (2007). An aluminum-activated citrate transporter in barley. Plant Cell Physiol. **48:** 1081–1091.

Gabetta, B., Fuzzati, N., Griffini, A., Lolla, E., Pace, R., Ruffilli, T., and Peterlongo, F. (2000). Characterization of proanthocyanidins from grape seeds. Fitoterapia **71:** 162–175.

Gomez, C., Terrier, N., Torregrosa, L., Vialet, S., Fournier-Level, A., Verriès, C., Souquet, J.M., Mazauric, J.P., Klein, M., Cheynier, V., and Ageorges, A. (2009). Grapevine MATE-type proteins act as vacuolar H^+-dependent acylated anthocyanin transporters. Plant Physiol. **150:** 402–415.

Goodman, C.D., Casati, P., and Walbot, V. (2004). A multidrug resistance-associated protein involved in anthocyanin transport in *Zea mays*. Plant Cell **16:** 1812–1826.

Grotewold, E. (2004). The challenges of moving chemicals within and out of cells: Insights into the transport of plant natural products. Planta **219:** 906–909.

Grotewold, E., Chamberlin, M., Snook, M., Siame, B., Butler, L., Swenson, J., Maddock, S., St. Clair, G., and Bowen, B. (1998). Engineering secondary metabolism in maize cells by ectopic expression of transcription factors. Plant Cell **10:** 721–740.

Gu, L., Kelm, M.A., Hammerstone, J.F., Beecher, G., Holden, J., Haytowitz, D., Gebhardt, S., and Prior, R.L. (2004). Concentrations of proanthocyanidins in common foods and estimations of normal consumption. J. Nutr. **134:** 613–617.

Hopp, W., and Seitz, H.U. (1987). The uptake of acylated anthocyanin into isolated vacuoles from a cell suspension culture of *Daucus carota*. Planta **170:** 74–85.

Jaquinod, M., Villiers, F., Kieffer-Jaquinod, S., Hugouvieux, V., Bruley, C., Garin, J., and Bourguignon, J. (2007). A proteomics dissection of *Arabidopsis thaliana* vacuoles isolated from cell culture. Mol. Cell. Proteomics **6:** 394–412.

Jørgensen, K., Rasmussen, A.V., Morant, M., Nielsen, A.H., Bjarnholt, N., Zagrobelny, M., Bak, S., and Møller, B.L. (2005). Metabolon formation and metabolic channeling in the biosynthesis of plant natural products. Curr. Opin. Plant Biol. **8:** 280–291.

Karimi, M., Inzé, D., and Depicker, A. (2002). GATEWAY vectors for *Agrobacterium*-mediated plant transformation. Trends Plant Sci. **7:** 193–195.

Kitamura, S. (2006). Transport of flavonoids: From cytosolic synthesis to vacuolar accumulation. In The Science of Flavonoids, E. Grotewald, ed (New York: Springer), pp. 123–146.

Kitamura, S., Matsuda, F., Tohge, T., Yonekura-Sakakibara, K., Yamazaki, M., Saito, K., and Narumi, I. (2010). Metabolic profiling and cytological analysis of proanthocyanidins in immature seeds of *Arabidopsis thaliana* flavonoid accumulation mutants. Plant J. **62:** 549–559.

Kitamura, S., Shikazono, N., and Tanaka, A. (2004). TRANSPARENT TESTA 19 is involved in the accumulation of both anthocyanins and proanthocyanidins in Arabidopsis. Plant J. **37:** 104–114.

Klein, M., Martinoia, E., Hoffmann-Thoma, G., and Weissenböck, G. (2000). A membrane-potential dependent ABC-like transporter mediates the vacuolar uptake of rye flavone glucuronides: Regulation of glucuronide uptake by glutathione and its conjugates. Plant J. **21:** 289–304.

Klein, M., Weissenböck, G., Dufaud, A., Gaillard, C., Kreuz, K., and Martinoia, E. (1996). Different energization mechanisms drive the vacuolar uptake of a flavonoid glucoside and a herbicide glucoside. J. Biol. Chem. **271:** 29666–29671.

Lee, Y., Yoon, H.R., Paik, Y.S., Liu, J.R., Chung, W.I., and Choi, G. (2005). Reciprocal regulation of Arabidopsis UGT78D2 and BANYULS is critical for regulation of the metabolic flux of anthocyanidins to condensed tannins in developing seed coats. J. Plant Biol. **48:** 356–370.

Lees, G.L. (1992). Condensed tannins in some forage legumes: Their role in the prevention of ruminant pasture bloat. Basic Life Sci. **59:** 915–934.

Lepiniec, L., Debeaujon, I., Routaboul, J.-M., Baudry, A., Pourcel, L., Nesi, N., and Caboche, M. (2006). Genetics and biochemistry of seed flavonoids. Annu. Rev. Plant Biol. **57:** 405–430.

Li, L., He, Z., Pandey, G.K., Tsuchiya, T., and Luan, S. (2002). Functional cloning and characterization of a plant efflux carrier for multidrug and heavy metal detoxification. J. Biol. Chem. **277:** 5360–5368.

Luo, J., et al. (2007). Convergent evolution in the BAHD family of acyl transferases: Identification and characterization of anthocyanin acyl transferases from *Arabidopsis thaliana*. Plant J. **50:** 678–695.

Luvisetto, S., and Azzone, G.F. (1989). Local protons and uncoupling of aerobic and artificial delta muH-driven ATP synthesis. Biochemistry **28:** 1109–1116.

Magalhaes, J.V., et al. (2007). A gene in the multidrug and toxic compound extrusion (MATE) family confers aluminum tolerance in sorghum. Nat. Genet. **39:** 1156–1161.

Marinova, K., Kleinschmidt, K., Weissenböck, G., and Klein, M. (2007a). Flavonoid biosynthesis in barley primary leaves requires the presence of the vacuole and controls the activity of vacuolar flavonoid transport. Plant Physiol. **144:** 432–444.

Marinova, K., Pourcel, L., Weder, B., Schwarz, M., Barron, D., Routaboul, J.-M., Debeaujon, I., and Klein, M. (2007b). The *Arabidopsis* MATE transporter TT12 acts as a vacuolar flavonoid/H^+-antiporter active in proanthocyanidin-accumulating cells of the seed coat. Plant Cell **19:** 2023–2038.

Markham, K.R., Gould, K.S., Winefield, C.S., Mitchell, K.A., Bloor, S.J., and Boase, M.R. (2000). Anthocyanic vacuolar inclusions—Their nature and significance in flower colouration. Phytochemistry **55:** 327–336.

Marrs, K.A., Alfenito, M.R., Lloyd, A.M., and Walbot, V. (1995). A glutathione *S*-transferase involved in vacuolar transfer encoded by the maize gene *Bronze-2*. Nature **375:** 397–400.

Matern, U., Heller, W., and Himmelspach, K. (1983). Conformational changes of apigenin 7-O-(6-O-malonylglucoside), a vacuolar pigment from parsley, with solvent composition and proton concentration. Eur. J. Biochem. **133:** 439–448.

Matern, U., Reichenbach, C., and Heller, W. (1986). Efficient uptake of flavonoids into parsley (*Petroselinum hortense*) vacuoles requires acylated glycosides. Planta **167:** 183–189.

Mathews, H., Clendennen, S.K., Caldwell, C.G., Liu, X.L., Connors, K., Matheis, N., Schuster, D.K., Menasco, D.J., Wagoner, W., Lightner, J., and Wagner, D.R. (2003). Activation tagging in tomato identifies a transcriptional regulator of anthocyanin biosynthesis, modification, and transport. Plant Cell **15:** 1689–1703.

Modolo, L.V., Blount, J.W., Achnine, L., Naoumkina, M.A., Wang, X., and Dixon, R.A. (2007). A functional genomics approach to (iso) flavonoid glycosylation in the model legume *Medicago truncatula*. Plant Mol. Biol. **64:** 499–518.

Morita, M., Shitan, N., Sawada, K., Van Montagu, M.C., Inzé, D., Rischer, H., Goossens, A., Oksman-Caldentey, K.M., Moriyama, Y., and Yazaki, K. (2009). Vacuolar transport of nicotine is mediated by a multidrug and toxic compound extrusion (MATE) transporter in *Nicotiana tabacum*. Proc. Natl. Acad. Sci. USA **106:** 2447–2452.

Mueller, L.A., Goodman, C.D., Silady, R.A., and Walbot, V. (2000). AN9, a petunia glutathione *S*-transferase required for anthocyanin sequestration, is a flavonoid-binding protein. Plant Physiol. **123:** 1561–1570.

Nawrath, C., Heck, S., Parinthawong, N., and Métraux, J.P. (2002). EDS5, an essential component of salicylic acid-dependent signaling for disease resistance in *Arabidopsis*, is a member of the MATE transporter family. Plant Cell **14:** 275–286.

Pang, Y., Peel, G.J., Sharma, S.B., Tang, Y., and Dixon, R.A. (2008). A transcript profiling approach reveals an epicatechin-specific glucosyltransferase expressed in the seed coat of *Medicago truncatula*. Proc. Natl. Acad. Sci. USA **105:** 14210–14215.

Peel, G.J., Pang, Y., Modolo, L.V., and Dixon, R.A. (2009). The LAP1 MYB transcription factor orchestrates anthocyanidin biosynthesis and glycosylation in Medicago. Plant J. **59:** 136–149.

Pezza, R.J., Villarreal, M.A., Montich, G.G., and Argaraña, C.E. (2002). Vanadate inhibits the ATPase activity and DNA binding capability of bacterial MutS. A structural model for the vanadate-MutS interaction at the Walker A motif. Nucleic Acids Res. **30:** 4700–4708.

Pfaffl, M.W. (2001). A new mathematical model for relative quantification in real-time RT-PCR. Nucleic Acids Res. **29:** e45.

Pourcel, L., Irani, N.G., Lu, Y., Riedl, K., Schwartz, S., and Grotewold, E. (2010). The formation of anthocyanic vacuolar inclusions in *Arabidopsis thaliana* and implications for the sequestration of anthocyanin pigments. Mol Plant **3:** 78–90.

Poustka, F., Irani, N.G., Feller, A., Lu, Y., Pourcel, L., Frame, K., and Grotewold, E. (2007). A trafficking pathway for anthocyanins overlaps with the endoplasmic reticulum-to-vacuole protein-sorting route in Arabidopsis and contributes to the formation of vacuolar inclusions. Plant Physiol. **145:** 1323–1335.

Ramakers, C., Ruijter, J.M., Deprez, R.H., and Moorman, A.F. (2003). Assumption-free analysis of quantitative real-time polymerase chain reaction (PCR) data. Neurosci. Lett. **339:** 62–66.

Rodrigues, C.O., Scott, D.A., and Docampo, R. (1999). Presence of a vacuolar H^+-pyrophosphatase in promastigotes of *Leishmania*

donovani and its localization to a different compartment from the vacuolar H^+-ATPase. Biochem. J. **340:** 759–766.

Santos-Buelga, C., and Scalbert, A. (2000). Proanthocyanidins and tannin-like compounds—Nature, occurrence, dietary intake and effects on nutrition and health. J. Sci. Food Agric. **80:** 1094–1117.

Shoji, T., Inai, K., Yazaki, Y., Sato, Y., Takase, H., Shitan, N., Yazaki, K., Goto, Y., Toyooka, K., Matsuoka, K., and Hashimoto, T. (2009). Multidrug and toxic compound extrusion-type transporters implicated in vacuolar sequestration of nicotine in tobacco roots. Plant Physiol. **149:** 708–718.

Skibola, C.F., and Smith, M.T. (2000). Potential health impacts of excessive flavonoid intake. Free Radic. Biol. Med. **29:** 375–383.

Springob, K., Nakajima, J., Yamazaki, M., and Saito, K. (2003). Recent advances in the biosynthesis and accumulation of anthocyanins. Nat. Prod. Rep. **20:** 288–303.

St. Pierre, B., and De Luca, V. (2000). Evolution of acyltransferase genes: Origin and diversification of the BAHD superfamily of acyltransferases involved in secondary metabolism. In Recent Advances in Phytochemistry. Vol. 34. Evolution of Metabolic Pathways, J.T. Romeo, R. Ibrahim, L. Varin, and V. De Luca, eds (Amsterdam: Elsevier), pp. 285–315.

Strack, D., and Wray, V. (1994). The anthocyanins. In The Flavonoids, J.B. Harborne, ed (Washington: Chapman & Hall/CRC Press), pp. 1–22.

Suzuki, H., Nakayama, T., and Nishino, T. (2003). Proposed mechanism and functional amino acid residues of malonyl-CoA:anthocyanin 5-*O*-glucoside-6′′-*O*-malonyltransferase from flowers of *Salvia splendens*, a member of the versatile plant acyltransferase family. Biochemistry **42:** 1764–1771.

Suzuki, H., Nakayama, T., Yonekura-Sakakibara, K., Fukui, Y., Nakamura, N., Yamaguchi, M.A., Tanaka, Y., Kusumi, T., and Nishino, T. (2002). cDNA cloning, heterologous expressions, and functional characterization of malonyl-coenzyme A:anthocyanidin 3-*O*-glucoside-6′′-*O*-malonyltransferase from dahlia flowers. Plant Physiol. **130:** 2142–2151.

Suzuki, H., Sawada, S., Watanabe, K., Nagae, S., Yamaguchi, M.A., Nakayama, T., and Nishino, T. (2004). Identification and characterization of a novel anthocyanin malonyltransferase from scarlet sage (*Salvia splendens*) flowers: An enzyme that is phylogenetically separated from other anthocyanin acyltransferases. Plant J. **38:** 994–1003.

Suzuki, R., and Shimodaira, H. (2006). Pvclust: An R package for assessing the uncertainty in hierarchical clustering. Bioinformatics **22:** 1540–1542.

Tadege, M., Wen, J., He, J., Tu, H., Kwak, Y., Eschstruth, A., Cayrel, A., Endre, G., Zhao, P.X., Chabaud, M., Ratet, P., and Mysore, K.S. (2008). Large-scale insertional mutagenesis using the Tnt1 retrotransposon in the model legume Medicago truncatula. Plant J. **54:** 335–347.

Taguchi, G., Ubukata, T., Nozue, H., Kobayashi, Y., Takahi, M., Yamamoto, H., and Hayashida, N. (2010). Malonylation is a key reaction in the metabolism of xenobiotic phenolic glucosides in Arabidopsis and tobacco. Plant J. **63:** 1031–1041.

Thompson, E.P., Wilkins, C., Demidchik, V., Davies, J.M., and Glover, B.J. (2010). An Arabidopsis flavonoid transporter is required for anther dehiscence and pollen development. J. Exp. Bot. **61:** 439–451.

Winkel, B.S.J. (2004). Metabolic channeling in plants. Annu. Rev. Plant Biol. **55:** 85–107.

Xie, D.Y., Sharma, S.B., Paiva, N.L., Ferreira, D., and Dixon, R.A. (2003). Role of anthocyanidin reductase, encoded by *BANYULS* in plant flavonoid biosynthesis. Science **299:** 396–399.

Yazaki, K. (2005). Transporters of secondary metabolites. Curr. Opin. Plant Biol. **8:** 301–307.

Yu, X.H., Chen, M.H., and Liu, C.J. (2008). Nucleocytoplasmic-localized acyltransferases catalyze the malonylation of 7-*O*-glycosidic (iso) flavones in *Medicago truncatula*. Plant J. **55:** 382–396.

Zhang, H., Wang, L., Deroles, S., Bennett, R., and Davies, K. (2006). New insight into the structures and formation of anthocyanic vacuolar inclusions in flower petals. BMC Plant Biol. **6:** 29.

Zhao, J., Connorton, J.M., Guo, Y., Li, X., Shigaki, T., Hirschi, K.D., and Pittman, J.K. (2009). Functional studies of split Arabidopsis Ca^{2+}/H^+ exchangers. J. Biol. Chem. **284:** 34075–34083.

Zhao, J., and Dixon, R.A. (2009). MATE transporters facilitate vacuolar uptake of epicatechin 3′-*O*-glucoside for proanthocyanidin biosynthesis in *Medicago truncatula* and *Arabidopsis*. Plant Cell **21:** 2323–2340.

Zhao, J., and Dixon, R.A. (2010). The 'ins' and 'outs' of flavonoid transport. Trends Plant Sci. **15:** 72–80.

Zhou, R., Jackson, L., Shadle, G., Nakashima, J., Temple, S., Chen, F., and Dixon, R.A. (2010). Distinct cinnamoyl CoA reductases involved in parallel routes to lignin in *Medicago truncatula*. Proc. Natl. Acad. Sci. USA **107:** 17803–17808.